JOURNAL OF GEOPHYSICAL RESEARCH, VOL. 104, NO. C9, PAGES 20,927–20,948, SEPTEMBER 15, 1999

Interannual variability of South Atlantic circulation from 4 years of TOPEX/POSEIDON satellite altimeter observations

Donna L. Witter and Arnold L. Gordon

Lamont-Doherty Earth Observatory, Columbia University, Palisades, New York

Abstract. Variability of large-scale and regional South Atlantic circulation is investigated using TOPEX/POSEIDON sea level observations. Interannual variations are identified from empirical orthogonal functions of gridded sea level fields, year-to-year fluctuations of root-mean-square sea level variability, and variability of Agulhas eddies evaluated from the along-track data. Two modes of variability are identified. A basin-scale mode indicates that sea level in the eastern South Atlantic underwent a transition from a state of high sea level and enhanced gyre-scale geostrophic circulation in 1993 and 1994, to a state of lower sea level and more sluggish circulation in 1996. The dominant mode of basin-scale zonal wind has the same temporal signature, suggesting a link between the observed variation of gyre-scale circulation and the regional wind forcing. Time variations of this mode also coincide with a transition from a broad Agulhas eddy corridor observed in 1993 and 1994 to a narrower corridor observed in 1996. The input of salt and vorticity to the South Atlantic subtropical gyre via Agulhas eddies may therefore be partially controlled by interannual variations of the wind-forced, large-scale circulation. A second mode isolates interannual variations in the Brazil-Malvinas Confluence region. During 1993, eddy variability along the Brazil Current extension was relatively strong and variability along the continental slope was weak. The opposite pattern was observed in 1995. These variations may be related to interannual variations of the latitude of the confluence. While variations associated with both modes are smaller than those observed on seasonal timescales, these interannual variations contribute significantly to the total South Atlantic variability.

1. Introduction

Like other midlatitude oceans, the dominant feature of South Atlantic circulation is anticyclonic flow around the subtropical gyre (see Figure 1). However, in the South Atlantic, this pattern of gyre-scale flow is particularly strongly influenced by interocean connections, which play an important role in the thermohaline circulation [*Reid,* 1989]. Interocean exchanges permit the thermohaline regimes of neighboring oceans to interact on a variety of timescales, from the high frequencies associated with mesoscale features, to seasonal, decadal, and lower frequencies. External forcing from neighboring ocean basins may induce variability in the South Atlantic boundary currents. This boundary current variability may, in turn, induce changes in the full South Atlantic subtropical gyre. Studies of the gyre-scale circulation and of low-frequency variability in the boundary current regimes may therefore provide insight to variations of the thermohaline circulation.

From a time-mean perspective (see Figure 1), the subtropical gyre of the South Atlantic acquires the coldest forms of sub-Antarctic mode water and Antarctic intermediate water from the Pacific inflow within Drake Passage. At the Brazil-Malvinas Confluence, the sharply contrasting circumpolar and South Atlantic thermocline waters form strong frontal features and energetic eddies [*Peterson and Stramma,* 1991]. Warm, saline thermocline water, a somewhat warmer, more saline form of sub-Antarctic mode water, and Antarctic intermediate water are drawn from the Indian Ocean at the Agulhas Retroflection. The interocean flux at the Agulhas Retroflection is accomplished by shedding of large rings or eddies of Indian Ocean water at the Agulhas Retroflection [*van Ballegooyen et al.,* 1994; *Lutjeharms,* 1996]. These eddies drift westward across the South Atlantic near 30°S [*Byrne et al.,* 1995]. In the Cape Basin, the Benguela Current thermocline water between the eddies is laced with Indian Ocean water [*Gordon et al.,* 1992], which may be introduced by filaments of Agulhas Current [*Lutjeharms and Cooper,* 1996] and by dissipation of Agulhas eddies [*Byrne et al.,* 1995; *Gor-*

Paper number 1999JC900023.
0148-0227/99/1999JC900023$09.00

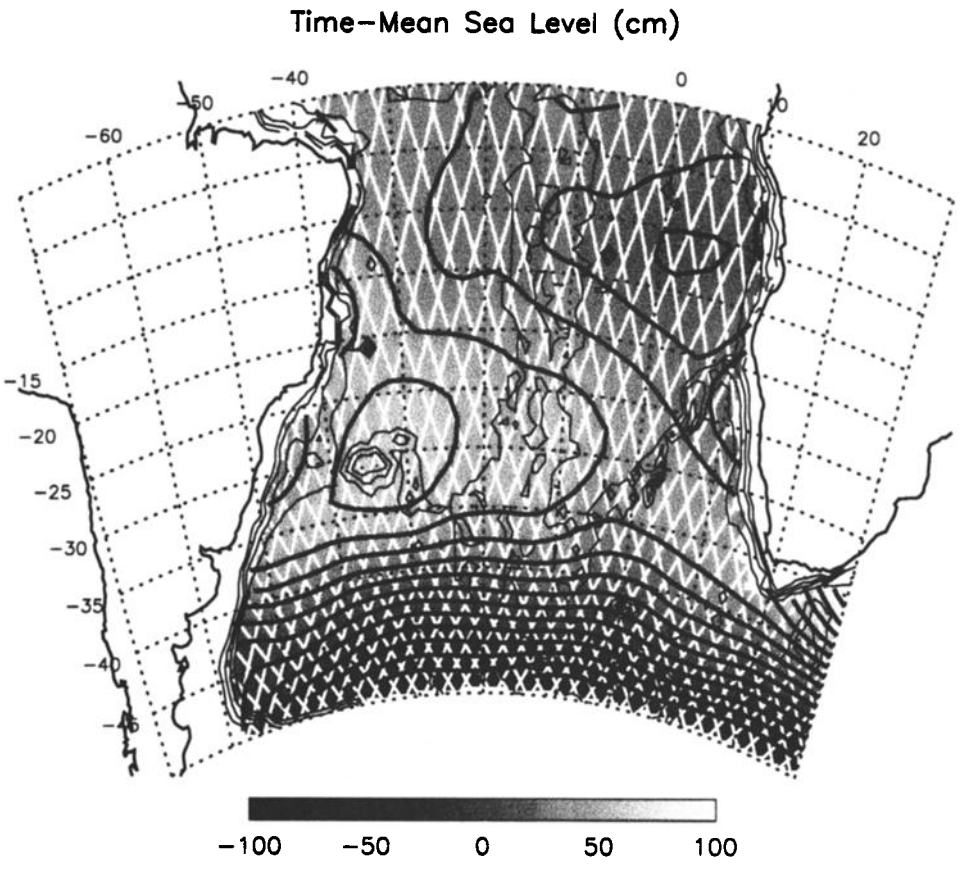

Figure 1. Time-mean dynamic height (shaded image and thick black contours) for the South Atlantic basin computed from TOPEX/POSEIDON (T/P) observations relative to the Joint Gravity Model 3 geoid. The dynamic height contour interval is 10 centimeters. Bathymetry contours are plotted as thin solid lines at 500 meter intervals. The T/P ground tracks are plotted as thin white lines. Note that the details of circulation in the boundary current regions (e.g., the Brazil-Malvinas Confluence and the Agulhas Retroflection) are not resolved by the smoother used to grid the time-mean field or by the geoid.

don, 1997]. The Benguela Current turns seaward as the South Equatorial Current, which bifurcates at the South American coast near 10°S in the surface layer and near 25°S at Antarctic intermediate water depths. The northward flowing branch within the North Brazil Coastal Current eventually crosses into the Northern Hemisphere, representing another vital interocean link of the South Atlantic.

Until recently, studies of the time-dependent variability of South Atlantic circulation have either focused on small regions or been based on short records of large-scale variability. Satellite data sets greatly improved this situation, particularly with regard to resolving large-scale, low-frequency variability [*Fu,* 1996]. Previous studies of South Atlantic circulation demonstrate that flow within this basin varies on a wide range of spatial and temporal scales. Geosat observations indicate that sea level near the Brazil-Malvinas Confluence varies on annual and semiannual cycles, with strongest eddy energy occurring in southern summer [*Provost and Le Traon,* 1993]. Estimates of the location of the Brazil-Malvinas Confluence inferred from Geosat altimetry indicate that the latitude of the confluence shifts by approximately 2° over the course of a year [*Matano et al.,* 1993]. The confluence reaches its most southerly (northerly) point in southern summer (winter) when the transport of the Brazil Current is strongest (weakest). This annual modulation may occur in response to seasonal shifts in the South Atlantic atmospheric high-pressure cell and seasonal variations in the transport of Antarctic Circumpolar Current water northward into the Malvinas Current [*Matano et al.,* 1993]. Semiannual and interannual variations of atmospheric pressure may produce similar modulations in regional ocean circulation; both *Matano et al.* [1993] and *Provost and Le Traon* [1993] note a difference in regional circulation inferred from each year of Geosat observations. A quantitative estimate of interannual variability is, however, difficult to obtain based on only 2 years of data.

In the Agulhas region, seasonal variations are weaker, possibly owing to the lack of a distinct annual cycle in the wind field [*Pearce and Gründlingh,* 1982]. Time-dependent variations in this region are more often attributed to semiannual variations of the wind [*Ffield et al.,* 1997] or to intermittent formation of eddies at the Agulhas Retroflection [*Garzoli and Gordon,* 1996]. Al-

timetric tracking of Agulhas eddies, analysis of thermal infrared imagery, and evaluation of hydrographic data suggest that between four and nine Agulhas eddies enter the South Atlantic each year [*Duncombe Rae et al.*, 1996]. The possibility of interannual fluctuations in Agulhas eddy transport cannot be ruled out [*Goni et al.*, 1997].

Low-frequency variations of Agulhas eddy production may have important ramifications for the thermohaline state of the South Atlantic Ocean. Water mass analysis demonstrates that these features contribute to the salinity balance of the Atlantic basin [*Gordon et al.*, 1992]. Variations in the production of Agulhas eddies may also induce time-dependent changes in the flux of eddy vorticity across the subtropical South Atlantic. As suggested by *Byrne et al.* [1995], this flux may contribute significantly to the vorticity budget of the Brazil Current, with the potential to affect rates of eddy formation and mixing at the Brazil-Malvinas Confluence. Such links between circulation in the eastern and western South Atlantic indicate that variations of South Atlantic circulation must be considered for the basin as a whole. The sampling provided by satellite altimetry is ideally suited for this task.

In this study, we analyze TOPEX/POSEIDON (T/P) sea level observations of the South Atlantic basin to improve understanding of the link between the large-scale and mesoscale components of the subtropical gyre circulation. This work addresses the following questions from an observational perspective: (1) What are the modes of low-frequency variability of the South Atlantic subtropical gyre? (2) Is there an apparent link between low-frequency variations of the gyre-scale circulation and low-frequency variations of mesoscale eddies? (3) Do low-frequency variations of the eastern and western boundary current regimes occur on the same timescales? (4) Within the eastern and western boundary currents, is there an apparent link between low-frequency variability of the boundary currents and low-frequency variability of mesoscale eddies?

One of the unique aspects of the T/P data set is the more than 4 years of observations currently available. The length and quality of the T/P data set is a substantial improvement over data available from previous altimeters [see *Fu et al.*, 1994]. The spatial and temporal coverage available from T/P is also far superior to that available from in situ sampling programs. The T/P database is extremely well suited for investigations of large-scale, low-frequency ocean variability.

The body of the paper is organized as follows. In section 2, we describe the T/P data set and our filtering techniques. In section 3, we describe the spatial and temporal variability of the basin-scale circulation and of circulation in the eastern and western boundary current regions using empirical orthogonal function (EOF) analysis. The frequency content and year-to-year changes of root-mean-square (rms) sea level variability are then presented in section 4. The contribution of Rossby wave propagation to variability in the interior of the South Atlantic subtropical gyre is discussed in section 5. Year-to-year variations of Agulhas eddy propagation in the interior of the gyre are discussed in section 6. An intriguing result of this analysis is an apparent relationship between variations of the large-scale gyre circulation and variations in the trajectories of Agulhas eddies. The role of wind forcing in this multiscale interaction is explored in section 7.

2. Data Processing

The T/P data used in this study are a processed version of the Merged Geophysical Data Records (MGDRs) obtained from V. Zlotnicki and A. Hyashi of the Jet Propulsion Laboratory. This data set was derived from the Physical Oceanography Distributed Active Archive Center (PO-DAAC) MGDRs (T/P cycles 1-132), the Archiving, Validation, and Interpretation of Satellite Data in Oceanography (AVISO) MGDRs (POSEIDON cycles following cycle 132), and the PO-DAAC Geophysical Data Records (TOPEX cycles following cycle 132). Along-track sea level residuals were computed from the Geophysical Data Records (GDRs) after applying the Joint Gravity Model 3 orbits and Rapp mean sea surface. Estimates of the ionospheric range delay, wet and dry tropospheric range delays, and inverse barometer effect were removed using corrections available on the GDRs. The TOPEX oscillator drift correction, pole tide correction, Gaspar 4.0 sea state bias correction, and a 147-mm TOPEX bias correction were also applied to the along-track sea level residuals. The resulting values were interpolated to a uniform along-track grid with 6.2-km spacing. Blunder points were identified and removed using the criteria described by *McClean et al.* [1997]. The final stages of preprocessing included (1) removing an estimate of the residual mean sea surface based on the time mean of 4 years of observations, (2) removing an estimate of the ocean tide contribution to sea level based on the University of Texas 3.0 tide model, and (3) removing energy at the frequencies of tidal aliases using the procedure described by *Schlax and Chelton* [1994, 1996]. The resulting along-track sea level anomalies for cycles 9–171 (December 1992 to May 1997) are our primary data set. Sea level values in regions shallower than 1000 m are excluded from the analysis.

Additional filtering is applied to the primary data set to isolate sea level variability on selected spatial and temporal scales. For all of the results described below, a one-dimensional loess filter [see *Schlax and Chelton*, 1992] was applied to eliminate variability with timescales shorter than about 30 days. For some of the analyses which follow, we use this temporally smoothed along-track data set directly; for other calculations it is more appropriate to work with a version of the data that can be mapped over the full South Atlantic domain. In the latter cases, we apply a two-dimensional loess spatial smoother [see *Greenslade et al.*, 1997] with either

a 6° or 12° half-span in latitude and longitude. The span of the filter is adjusted in the zonal direction by dividing by the cosine of latitude to account for convergence of the meridians. With this adjustment, the 6° and 12° smoothers are approximately equivalent to box averages over 400 and 800 km. respectively. Unlike a box average, however, the loess smoother has small sidelobes in the wavenumber domain and a smooth roll-off in latitude and longitude. In addition, uncertainty in the smoothed fields is nearly spatially and temporally homogeneous [*Greenslade et al.*, 1997]. As part of the smoothing procedure, the sea level fields are interpolated onto the 1.875° longitude by 1.9° latitude grid used by the National Center for Environmental Prediction/National Center for Atmospheric Research (NCEP/NCAR) Reanalysis Project [*Kalnay et al.*, 1996].

As discussed by *Stammer* [1997], altimeter-measured sea level variations can arise from dynamic changes of the position or intensity of ocean currents, via the geostrophic relation, or from changes of sea level due to thermal expansion of the near-surface layer. For this study, we are most interested in the former. Unfortunately, modeling the latter component of sea level variability requires high-resolution observations of air-sea fluxes [*Stammer*, 1997] or direct measurements of temperature variability within the upper layers of the ocean. Measurements of these quantities are generally sparse in the South Atlantic subtropical gyre, and the resulting estimates of steric expansion are of poor quality. In the analyses below, we remove an annual harmonic fit to sea level at each location to reduce the contribution of steric expansion to the total sea level variability. The zonal average is then removed at each time to reduce thermal residuals that cannot be modeled as a simple annual cycle. This procedure removes any dynamical variations of sea level on annual timescales, as well as the zonally uniform component of steric variability on interannual and other timescales. Because annual variability represents a significant fraction of the total sea level variability of the South Atlantic [*Chelton et al.*, 1990], the filtered data set is well suited for studying the less energetic, interannual variations of interest to this study. The contribution of residual steric effects to interannual variations of sea level is discussed, as appropriate, below.

3. Modes of Sea Level Variability

In this section, we present modes of sea level variability computed from EOF analysis of the gridded sea level fields [see *Preisendorfer*, 1988]. Gyre-scale modes are computed from sea level observations smoothed with the 12° loess filter. This filter removes much of the variability associated with small-scale features such as Agulhas eddies and Rossby waves. A separate analysis is also presented for the eastern and western boundary current regions based on observations gridded with the 6° loess smoother. This smoother facilitates recovery of the smallest possible spatial scales, given the T/P ground track configuration, with the requirement that errors in the smoothed fields are approximately statistically homogeneous [*Greenslade et al.*, 1997]. For both the large-scale and regional analyses, results are presented for the first two EOF modes; interpreting variability associated with higher order modes is difficult owing to the orthogonality constraint central to EOF analysis [see *Preisendorfer*, 1988].

3.1. Basin-Scale EOF Modes

For the full South Atlantic basin, the first EOF mode (Plate 1) accounts for 54% of the variance in the filtered sea level fields. The spatial pattern for this mode (Plate 1, top left) corresponds to changes of the large-scale circulation of the subtropical gyre. Anomalously high sea level occurs over the eastern third of the gyre at times when sea level is anomalously low near the western boundary. Temporal variations (Plate 1, bottom left) of geostrophic velocity associated with mode 1 indicate enhanced circulation in the eastern South Atlantic in 1993 and 1994, followed by a transition in mid-1995 through mid-1996 to a state of more sluggish flow. The location of maximum sea level anomalies in the eastern part of the domain (i.e., the reversed "C"-shaped pattern) corresponds well with the time-mean location of the eastern limb of the gyre (Figure 1). This mode therefore represents interannual variations in the zonal extent of the region of strong subtropical gyre circulation. The dome of sea level associated with the gyre is broad and flat in 1993 and 1994, when the gyre is displaced to the east of its time-mean position. During these years, the component of the Brazil Current associated with mode 1 is weaker than normal owing to the reduced zonal sea level gradient in the eastern third of the gyre. The dome of sea level associated with the gyre is taller and shifted toward the western boundary in 1996. The smoothed signature of Brazil Current velocities associated with mode 1 are correspondingly larger in 1996.

As noted above, sea level variations may be the result of dynamic changes of surface geostrophic currents or the result of local steric expansion. When interpreting large-scale sea level variations, such as those shown in Plate 1, it is important to estimate the contribution of steric expansion to the observed signal. This calculation requires accurate estimates of the upper layer thermal structure or accurate estimates of air-sea heat fluxes [see *Stammer*, 1997]. In the South Atlantic subtropical gyre, the network of in situ observations is spatially and temporally sparse and interannual variations of temperature at gyre scales are poorly resolved from in situ observations alone. As an alternative, we use a recently updated version of the *Reynolds and Smith* [1994] sea surface temperature (SST) data set, in conjunction with a simple model of vertical temperature anomalies, to estimate the interannual steric expansion of the gyre. Because the Reynolds and Smith data set

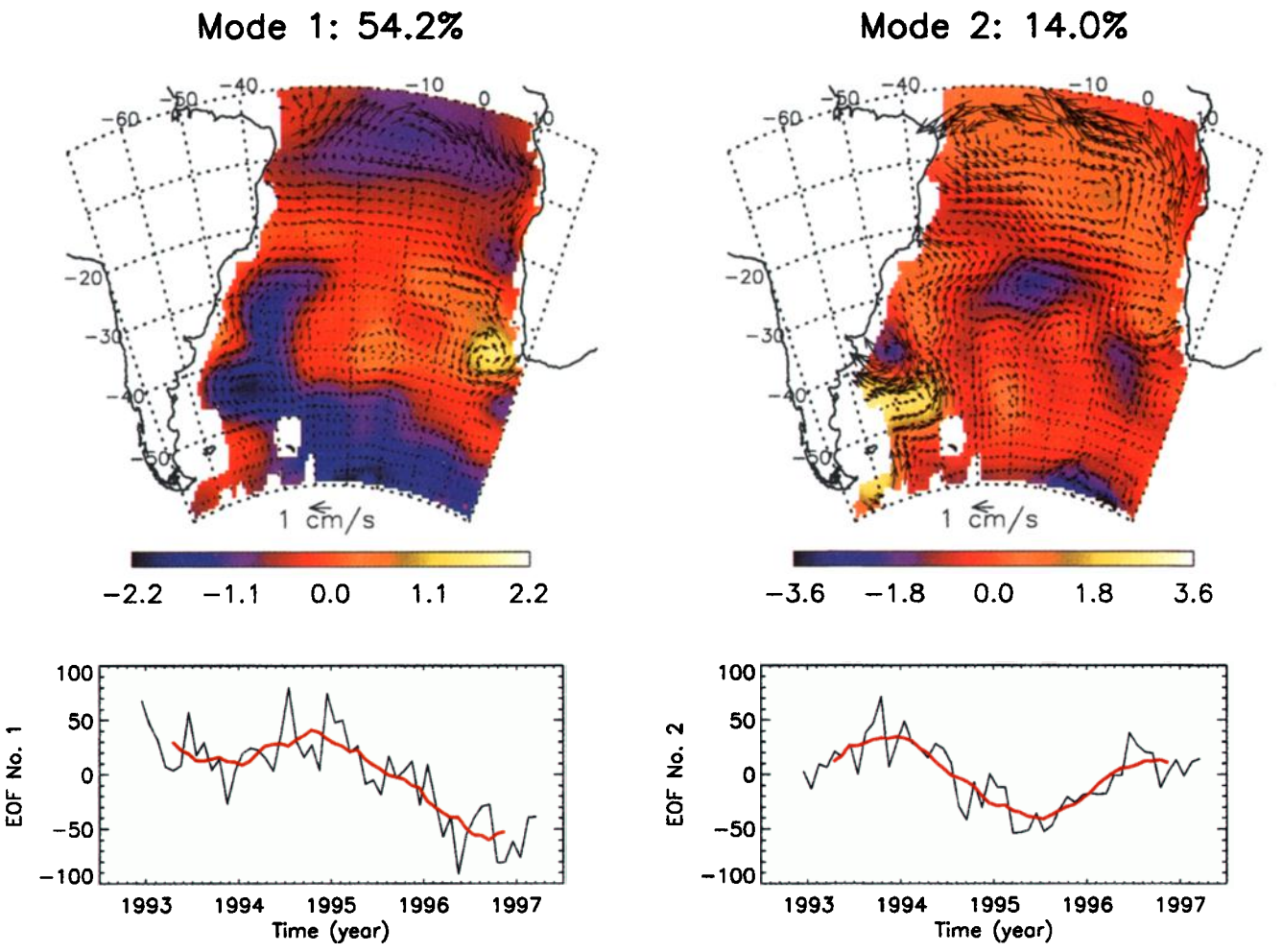

Plate 1. (top) Spatial patterns of the first two basin-scale sea level modes (color images), the corresponding geostrophic velocity fields (vectors), and (bottom) amplitude time series (black lines). The color bar indicates the sea level (in centimeters) when the amplitude time series is equal to 30.0. The 9-month running average of the amplitude time series is plotted in red (bottom).

includes both in situ and satellite observations, it is one of the best sources for studying interannual variations of the large-scale temperature field.

The interannual component of gyre-scale steric expansion is estimated based on modes of nonseasonal SST variability computed for the period contemporaneous with the T/P mission. After removing an annual and a semiannual harmonic at each location, EOF modes of SST variability were computed for the South Atlantic basin. Of the leading-order modes shown in Figure 2, the spatial pattern of mode 2 (15% of nonseasonal SST variability) is most strongly correlated with the spatial pattern of sea level mode 1 (ρ=0.59). The thermal expansion corresponding to the maximum low-frequency temperature change of SST mode 2 (1.2°C peak-to-peak) was computed assuming two profiles of vertical temperature anomaly. If an exponential decrease of temperature with depth with an e-folding scale of 100 m is assumed, the resulting peak to peak, low-frequency steric expansion is equivalent to a 2.2-cm peak-to-peak sea level variation. If a constant temperature anomaly between the surface and 200 m is assumed, the resulting low-frequency steric expansion is equivalent to a 3.8-cm peak-to-peak sea level variation. These values can be compared with the peak-to-peak, low-frequency sea level change of 7.6 cm observed for mode 1. While it is difficult to assess the degree to which these particular temperature anomaly profiles represent true variations of South Atlantic temperature on interannual timescales, the profiles assumed here are comparable to interannual variations of temperature observed in the less sparsely sampled North Pacific subtropical gyre. The maximum peak-to-peak variation of near-surface temperature in the North Pacific subtropical gyre is approximately 2°C on decadal timescales and about 1.2°C on year-to-year timescales [*Deser et al.*, 1996]; low-frequency temperature anomalies in the North Pacific subtropical gyre are vertically coherent within the upper 150–250 m of the water column [see *Deser et al.*, 1996, Figure 7]). Thus a relatively simple estimate of steric variations suggests that between 30% and 50% of the mode 1 sea level signal is the result of thermal expansion and the remaining

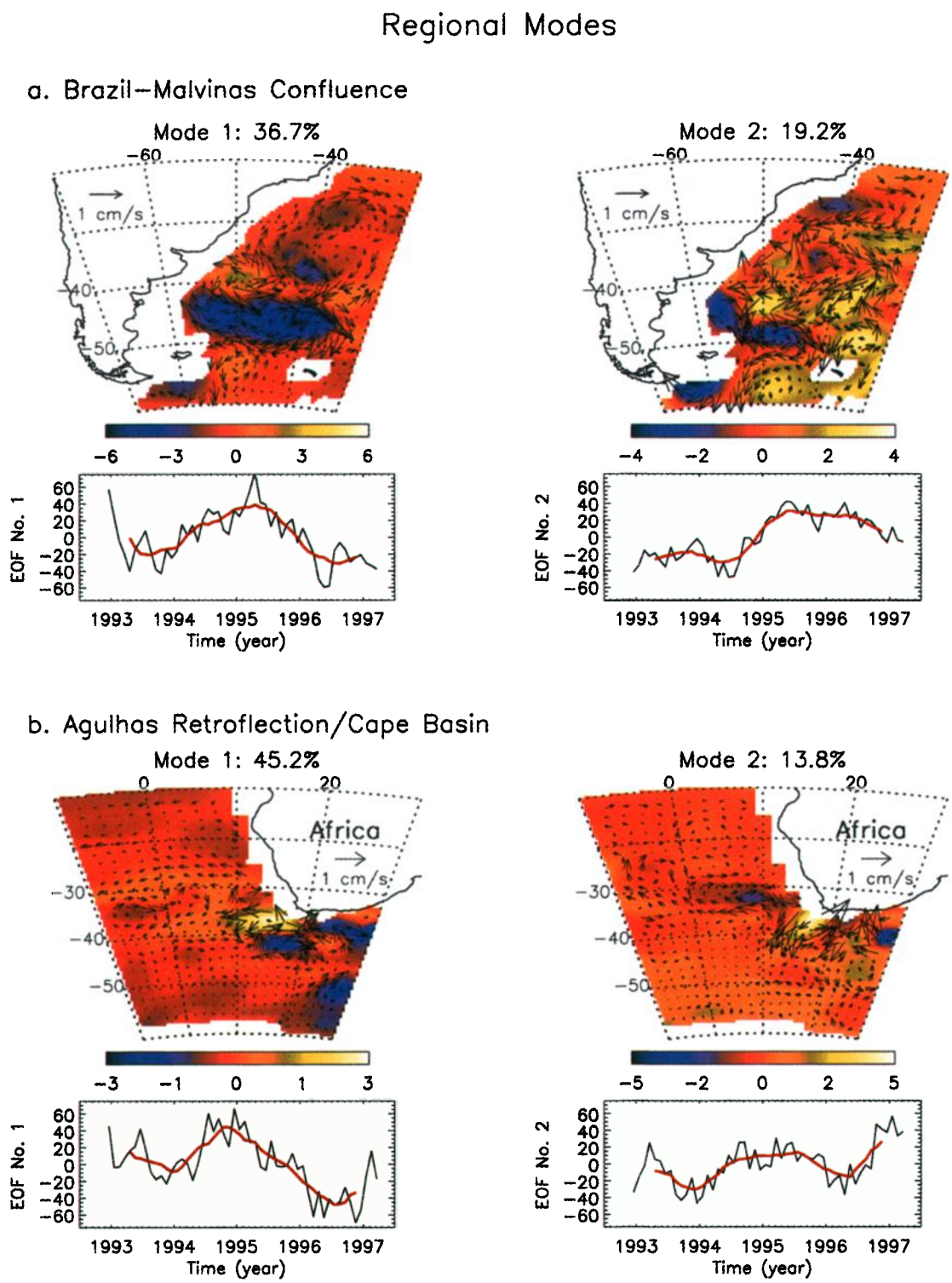

Plate 2. Regional empirical orthogonal function (EOF) modes for (a) the Brazil-Malvinas Confluence region and (b) the Agulhas Retroflection and Cape Basin region. The panels in Plate 2a and Plate 2b are laid out as in Plate 1. The color scale indicates sea level (in centimeters) when the amplitude time series is equal to 30 (Plate 2a) and 20 (Plate 2b).

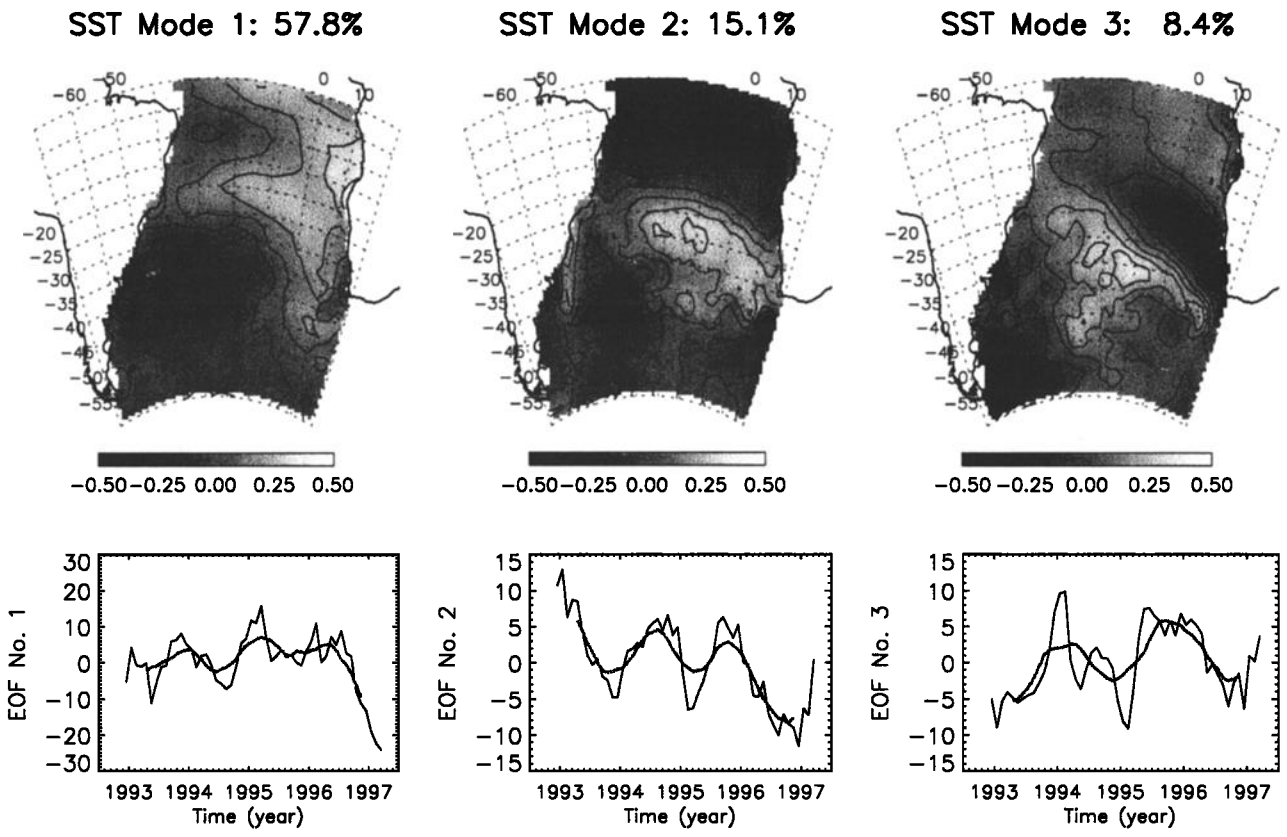

Figure 2. (top) Spatial patterns of the first three modes of basin-scale sea surface temperature (SST) variability (gray scale image and contours) and (bottom) their corresponding amplitude time series (solid lines). The gray-scale bar indicates SST in degrees Celsius when the amplitude time series is equal to 5.0. The amplitude time series smoothed with a 9-month running average (bottom, thick lines) shows the low-frequency component of variability associated with each mode. The good correspondence between the spatial pattern of SST mode 2 and the sea level pattern in Plate 1 (top left) suggests that SST mode 2 represents the steric contribution to sea level mode 1.

50–70% of mode 1 sea level variability can be attributed to variations of gyre-scale ocean circulation.

Inspection of the amplitude time series associated with sea level mode 1 and SST mode 2 suggests that the actual contribution of steric expansion to mode 1 sea level variability may be smaller than 30–50%. On low frequencies, the amplitude time series of sea level mode 1 and SST mode 2 are quite distinct. While sea level mode 1 and SST mode 2 both include secular trends, the dominant signal in the SST time series is a low-frequency oscillation; a comparable signature is not observed in the mode 1 sea level time series. The dominant feature of the mode 1 sea level time series (i.e., the strong transition during 1995, which separates the relatively uniform response in 1993-1994 from the response in 1996) has no counterpart in the SST time series. Because these low-frequency signals are very different, a larger estimate of the steric contribution to sea level mode 1 is not obtained by considering nonzero temporal lags.

On the basis of these comparison with SST EOFs, we conclude that while the gyre-scale response of sea level mode 1 includes a significant steric component, the larger contribution to this mode is the result of variations in ocean currents. Separating the thermal and dynamic components of ocean circulation is, however, somewhat artificial. Thus we cannot rule out the possibility that some of the correlation between sea level mode 1 and SST mode 2 may arise from advection of temperature anomalies by low-frequency variations of ocean circulation.

A second aspect of the modal analysis that must be considered carefully is the possible effect of aliasing on the mode structure. This is particularly important for sea level mode 1, which has large amplitudes near the Cape Basin. Sensitivity studies demonstrate that the 12° filter significantly attenuates small-scale features, including Agulhas eddies. This can be demonstrated quantitatively by setting sea level anomalies associated with the Agulhas eddies (see section 6) to zero in the along-track data. The resulting data set was then gridded and smoothed with the 12° filter, and basin-scale EOFs were calculated. The spatial patterns and time series of the leading-order EOFs match those displayed in Plate 1 nearly perfectly (that is, the lag 0 temporal correlation between the two mode 1 amplitude time series and the correlation between the two mode 1 spatial patterns are both equal to 0.92). As expected, remov-

ing small-scale variability associated with Agulhas eddies increases the percentage of variance explained by sea level mode 1 from 54% to 71%.

In situ observations of the large-scale South Atlantic circulation that might confirm the change of gyre circulation implied by mode 1 are not yet available for the full transition period (mid-1995 through mid-1996). For the period between October 1992 and September 1995, an analysis of in situ and satellite observations for the southeastern Atlantic shows little change of Benguela Current transport on interannual timescales [*Garzoli et al.*, 1997]; this period coincides with the interval of approximately constant amplitude for the mode 1 time series shown in Plate 1. As noted by *Garzoli et al.* [1997], variability of southeast Atlantic transport from late 1992 through mid-1995 corresponded to the passage of Agulhas rings rather than to variations in the larger-scale circulation.

Sea level variations associated with mode 2 account for 14% of the variance in the smoothed fields. As shown in Plate 1 (right), this mode represents primarily interannual fluctuations of regional circulation near the Brazil-Malvinas Confluence. Surface geostrophic velocities associated with mode 2 suggest a gradual decrease in the strength of the Malvinas Current between late 1993 and mid-1995, followed by an increase in the strength of the Malvinas Current through early 1997. Circulation around the sea level feature between 35°S and 40°S near the western boundary is consistent with this interpretation; the increase of anticyclonic circulation between 1993 and 1995 implies a southward displacement of the Brazil-Malvinas Confluence. Similar displacements, on seasonal timescales, have been attributed to reductions of Malvinas Current transport, relative to Brazil Current transport [*Matano et al.*, 1993]. The spatial pattern of this mode and its possible relationship to variability in the boundary current eddy field are considered in more detail in sections 3.2 and 4.2.

The patterns of basin-scale interannual variability represented by modes 1 and 2 have not been observed previously. This is due, in part, to the lack of observations that resolve low-frequency fluctuations of the gyre-scale circulation. The 4-year T/P data set provides an unprecedented opportunity to estimate the relative amplitude of interannual and seasonal variations on large spatial scales. As noted above, the annual cycle was removed in the analysis of basin-scale circulation to facilitate extraction of lower-frequency variations. If the annual cycle is retained, the leading EOF mode is primarily an annual signal that accounts for 57% of the variance in the smoothed sea level fields. Modes with spatial and temporal structures similar to the nonseasonal modes 1 and 2 then account for a significant fraction of the total sea level variance (20% and 10%, respectively). This comparison demonstrates the significance of low-frequency fluctuations in the South Atlantic basin. Low-frequency variability is also evident from year-to-year changes in the amplitude of the annual pattern isolated as the dominant mode of total sea level variability. The amplitude of this annual cycle is approximately 40% larger in 1993 and 1996 than in 1994 and 1995. This variation of annual amplitude is consistent with previous analyses of data from the Geosat Exact Repeat Mission. Using a similar methodology, *Chelton et al.* [1990] showed that leading-order modes of South Atlantic circulation represented variations on seasonal timescales but that the amplitude and phase of the seasonal cycle differed between 1987 and 1988. This comparison of the modes of basin-scale variability computed with and without the annual cycle demonstrates that there are two types of interannual variations in South Atlantic sea level. First, modes of interannual variability account for a significant fraction of the total South Atlantic sea level variance. Second, year-to-year variations in the amplitude of the South Atlantic seasonal cycle are quite large.

3.2. Regional EOF Modes

Time-dependent variations of circulation at the eastern and western boundaries are evaluated in this section using regional EOF analyses. For these calculations, a 6° loess smoother is applied to the sea level observations to obtain fields that include sea level variations on scales larger than about 3.6° (400 km). As in the gyre-scale calculations discussed above, interannual variations contribute significantly to the principal components in both boundary current regions. Near the Brazil-Malvinas Confluence, the regional modes are dominated by small-scale recirculation cells (Plate 2a). The two lowest-order regional modes can be interpreted as a high-resolution decomposition of basin-scale mode 2 (Plate 1, right). The anticyclonic circulation cell evident in regional mode 1 near 38°S, 50°W has previously been observed in geostrophic velocity estimates from a 15-month deployment of moored inverted echo sounders (IES) [*Garzoli*, 1993]. Cyclonic flow around the local minima of sea level anomaly near 36°S, 44°W and 46°S, 52°W was also apparent in the IES data set [*Garzoli*, 1993].

Geostrophic velocity anomalies reconstructed from the first two regional modes show that the small-scale circulation features are related to low-frequency variations in the latitude of the Brazil-Malvinas Confluence. The anomalously northward meridional velocities near the South American coast in 1993 and 1996 (Figure 3) are consistent with a northward displacement of the confluence. At these times, anticyclonic circulation around the feature near 38°S, 50°W was particularly strong (see Plate 2a, top left) and the Malvinas Current followed a relatively northward trajectory into the interior of the gyre. During 1995, the opposite situation occurred; the confluence was located south of its time-mean position and the extension of the Malvinas Current followed a more zonal path into the gyre interior.

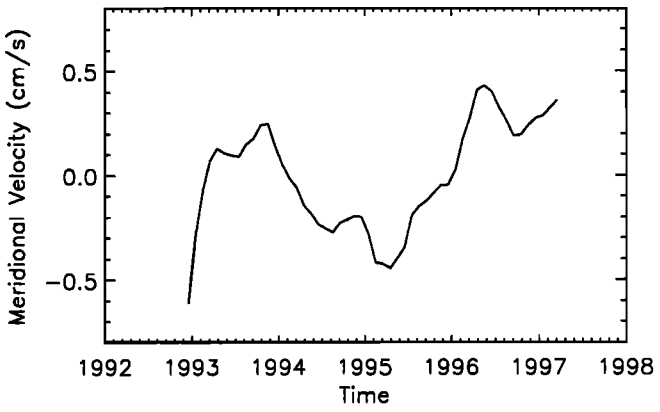

Figure 3. Spatially averaged meridional velocity for the region 305°E–310°E, 35°S-40°S. The time series is reconstructed from the first two regional empirical orthogonal functions (EOFs) from the Brazil-Malvinas Confluence (see Plate 3).

Near the Agulhas Retroflection, the first two regional modes (Plate 2b) have significant nonzero amplitudes only in the vicinity of the Agulhas Current and Agulhas Retroflection. Sea level anomalies reconstructed from these two modes are the result of the production of Agulhas eddies and the propagation of these eddies into the eastern Cape Basin. This process is illustrated by sea level time series reconstructed at the locations shown in Figure 4; as expected from Agulhas eddy propagation, sea level variations near the retroflection lead those to the north and west. Because the smoother used to generate the regional EOF modes damps sea level signatures associated with mesoscale features, the low-frequency variations in Plate 2b and Figure 4 should not be interpreted as the signatures of individual eddies. Instead, this variability represents a low-pass-filtered version of the convolution of the rate of eddy production and the amplitude of individual eddies. Note that low-frequency variability evident in the three reconstructed sea level time series (Figure 4) corresponds well with low-frequency variations of Agulhas eddy transport estimated based on assimilation of T/P data into a two-layer ocean model of the eastern South Atlantic [see *Goni et al.*, 1997, Figure 7].

In both boundary current regions, interannual variability is a significant fraction of the total sea level variability over the 4 years considered here. If the annual cycle is retained, annual variability in the Brazil-Malvinas Confluence region occurs as the dominant mode, accounting for 48% of the total variance; the regional modes displayed in Plate 2a then account for 19% and 9% of the total variability, respectively. Interannual variations have previously been observed in the separation latitudes of the Brazil and Malvinas Currents [*Olson et al.*, 1988], in the transport of the Brazil Current [*Garzoli*, 1993], and in the transport of the Malvinas Current [*Matano et al.*, 1993]. The results shown here demonstrate the regional nature of this interannual variability. Significant interannual fluctuations occur along

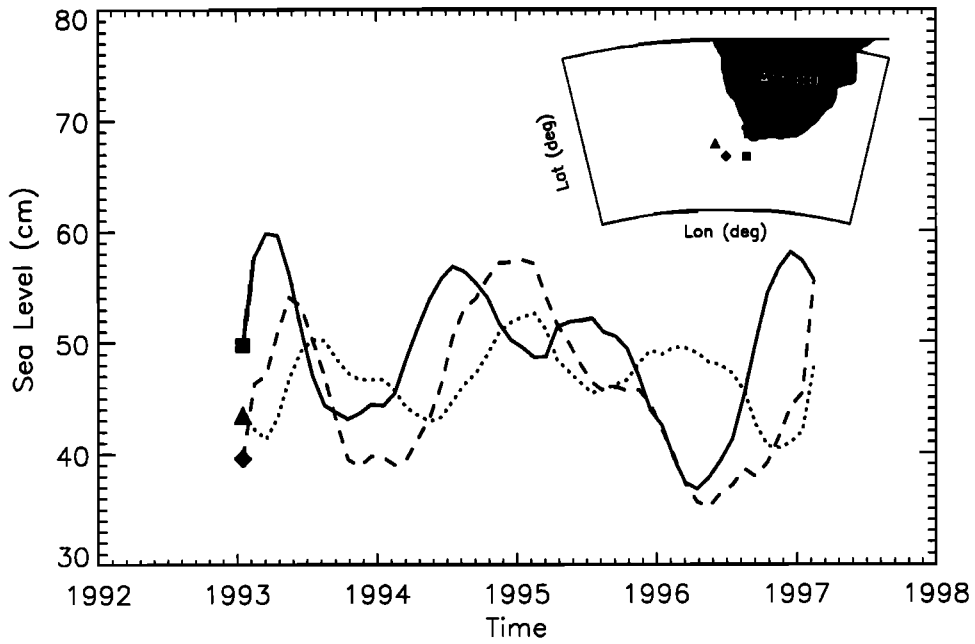

Figure 4. Sea level time series reconstructed from the first two regional modes of the Agulhas Current and Cape Basin regions. Sea level time series are plotted for the three locations shown in the map inset, 37°S, 19°E (solid line), 37°S, 15°E (dashed line), and 35°S, 13°E (dotted line). The lagged cross correlation between the solid and dashed lines reaches a maximum of 0.81 for a 2-month lag. The lagged cross correlation between the solid and dotted lines reaches a maximum of 0.66 for a 6-month lag. These correlations suggest that modes 1 and 2 are related to the propagation of Agulhas eddies from the retroflection into the Cape Basin.

the entire western boundary; variability in one part of the regional circulation is closely linked to variability in other elements of the regional circulation.

In the Agulhas Retroflection region, in situ and satellite observations suggest that annual variability is present [*Ffield*, 1997; *Matano et al.*, 1998], but weak [*Pearce and Gründlingh*, 1982]. This observation is supported by the T/P measurements. If the annual cycle is retained, the first and second modes displayed in Plate 2b account for 33% and 13% of the variability, respectively, while the annual cycle accounts for 21% of the variance. Unlike the western boundary region, interannual variability near the eastern boundary of the gyre is strongly localized. For the scales considered here, significant interannual variations are observed only at the retroflection and along the Agulhas eddy corridor within the eastern Cape Basin. As shown in section 6, interannual variability does occur in other regions of the Cape Basin, but this variability is restricted to scales that are not resolved by the 6° filter.

4. The rms Variability

Geographic and time-dependent changes of ocean variability also can be inferred from root-mean-square (rms) variations of altimeter-measured sea level. Variability in the South Atlantic basin is investigated here from rms height variations in three frequency bands and from a comparison of high-frequency rms variability in boundary current regions for each year of the T/P mission. To maintain consistency with other calculations presented in this paper, an annual harmonic is first removed at each along-track point. For the band-passed calculations, the rms variability at each along-track point is computed for timescales less than 4 months, between 4 and 12 months, and longer than 12 months. Year-to-year changes of regional rms variability are inferred from statistics of sea level variations along each ground track for 1993, 1994, 1995, and 1996. The band-passed and yearly rms variability fields are then mapped to a regular longitude-latitude grid using a smoother that retains variability on scales longer than about 150 km.

4.1. Band-Passed rms Variability

Because mesoscale motions associated with frontal instabilities are highly energetic, rms variability on short timescales is largest in the boundary current regions (Figure 5, left). At the Brazil-Malvinas Confluence, patches of locally high rms variability are associated with meandering of the Brazil and Malvinas Currents and with the production of mesoscale eddies at their confluence. Variability associated with meandering of the Agulhas and Agulhas Return Currents dominates the high-frequency rms variability near the eastern boundary of the subtropical gyre. Effects of Agulhas eddy propagation from the retroflection into the Cape Basin appear as a northwestward extension of the region of high variability between 20°E and 5°E. At high frequencies, rms sea level variations at the interior of the gyre are at least a factor of 5 smaller than those associated with the boundary currents.

On longer timescales, rms variations at the interior of the gyre are more comparable to variations in the boundary current regions (Figure 5, middle and right). As discussed in sections 5 and 6, sea level fluctuations on these longer timescales can be attributed to Rossby wave propagation and propagation of Agulhas eddies from the retroflection into the gyre interior. For timescales between 4 and 12 months, the maximum of

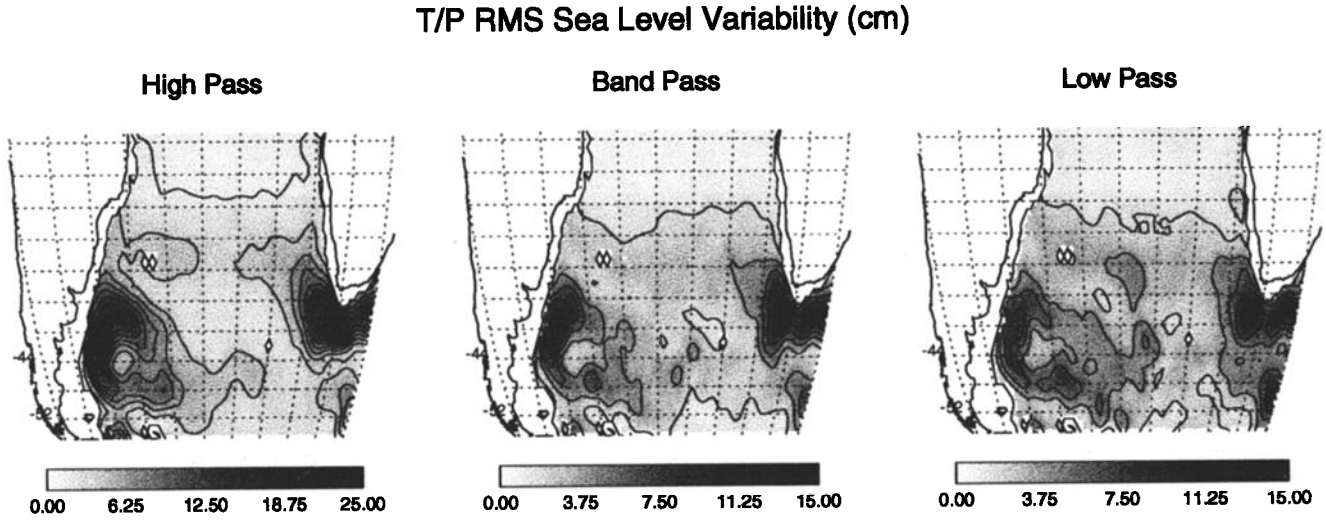

Figure 5. Filtered root-mean-square (rms) sea level variability from cycles 9–171 of the T/P mission. Filter parameters are set to extract high, intermediate, and low frequencies (more than 1 cycle per 4 months, 1 cycle per 4 months to 1 cycle per year, and less than 1 cycle per year, respectively). The contour interval is 2 centimeters; note the change of gray scale between the high-pass and band-pass filters. An estimate of the annual cycle is removed from the altimeter heights prior to calculating rms variability.

variability near the confluence of the Brazil and Malvinas Currents agrees with previous observations of eddy energy in the Brazil Basin, including observations of energetic semiannual variations of the Brazil Current and the latitude of the Brazil-Malvinas Confluence [*Forbes et al.*, 1993; *Le Traon and Minster*, 1993; *Provost and Le Traon*, 1993]. Variability along the convergence of the subpolar and sub-Antarctic fronts of the Antarctic Circumpolar Current at 48°S occurs predominantly on timescales longer than 1 year.

4.2. Year-to-Year Variations of Regional Variability

In the Brazil-Malvinas Confluence region, both the amplitude and the structure of the high-frequency variability change from year to year (Plate 3a). The general pattern of variability includes (1) a zonally oriented band of high variability located at approximately 38°S along the offshore extension of the Brazil Current, (2) a zonally oriented band of high variability along approximately 48°S, and (3) a meridional band of high variability in the boundary current region between 38°S and 48°S [also see *Fu*, 1996].

For the 4 years considered here, the maximum gridded rms variability near the Brazil-Malvinas Confluence reached 0.25, 0.25, 0.30, and 0.27 m in 1993, 1994, 1995, and 1996, respectively. The rms variability patterns for 1994 and 1996 most closely match the 4-year averaged pattern. Over the 4-year period evaluated here, the location of the maximum of rms variability shifted to the south and east; the maximum was located at 50°W, 40°S in 1993. By 1996, the maximum was located near 53°W, 42°S.

An intriguing aspect of the year-to-year changes of rms variability are the apparent low-frequency variations in the locations of high eddy energy. In 1993 and 1994, the region of strong eddy variability was broad and projected far to the east (i.e., into the offshore extension of the Brazil Current). In 1995, the maximum of variability was spatially compact and located adjacent to the continental slope. Variability in the offshore extension of the Brazil Current was about 20–25% smaller in 1995 than in 1993 or 1994. Variability in the region adjacent to the continental slope was about 20% larger in 1995 than in 1993 or 1994. During 1996, the region of high variability expanded and variability increased along the Brazil Current extension. These shifts in the spatial distribution of eddy energy coincide with variations of regional circulation inferred from the EOF analysis. As noted in section 3, the low-frequency variations of boundary current circulation are consistent with a apparent shift in the latitude of the confluence on a timescale of 2–3 years. During 1995 the confluence was located particularly far to the south. The yearly maps of rms variability shown in Plate 3a suggest that this displacement of the confluence coincides with a reduction in the amplitude of variability along the Brazil Current extension and with a localization of eddy variability adjacent to the continental slope.

A more subtle aspect of the low-frequency regional variability is the distribution of eddy energy along the convergence of the sub-Antarctic and subpolar fronts of the Antarctic Circumpolar Current (i.e., along 48°S). The longitude of maximum variability in this convergence zone shifts from year to year, occupying its westernmost position in 1995 and its easternmost position in 1993. With only 4 years of observations and few supporting in situ measurements, relating these variations to properties of the large-scale circulation is difficult. It is, however, intriguing that the local maximum of sea level variability is located farther west in years when the Brazil-Malvinas Confluence is located farther south. The possible role of the latitude of the confluence on eddy variability at 48° is consistent with results from a 14-month deployment of current meters northeast of the Ewing Bank between 47°S and 49°S along 41°W; eddy variability increased at the array when the offshore extension of the Malvinas Current shifted to the south [*Whitworth et al.*, 1991].

Near the eastern boundary (Plate 3b), high-frequency variability is the result of several processes [see *Duncombe Rae*, 1991]. Meandering and the formation of instabilities produce particularly strong variability along the Agulhas Return Current. Agulhas eddy production contributes to a region of strong variability near the westernmost extension of the retroflection. The westward propagation of eddies into the Cape Basin contributes to high variability within the Cape Basin. Plate 3b demonstrates that year-to-year changes of rms variability are relatively large in the eastern Cape Basin. These changes correlate well with year-to-year variations in the number of Agulhas eddies tracked from the Cape Basin into the interior of the gyre (see section 6).

The "patchiness" of variability near the Agulhas Retroflection appears to be correlated with the underlying topography. In 3 of the years shown in Plate 3b (1993, 1995, and 1996), a local minimum of variability is observed directly above the Agulhas Plateau (26°E). In 1994, a smaller, but still distinct gap in the eddy variability distribution is observed along the eastern flank of the plateau. The region of high variability located to the west of the plateau coincides with the most commonly observed position of the Agulhas Retroflection (16–20°E) [*Lutjeharms and van Ballegooyen*, 1988]. The secondary region of high variability located east of the plateau coincides with the region of high variability associated with meandering along the Agulhas Return Current. This region of locally intense eddy energy may also coincide with variability associated with the less frequently observed "early" position of the retroflection (i.e., cases where the retroflection occurs near 25°E) [*Lutjeharms and van Ballegooyen*, 1988]. The rms variability fields from 1993, 1995, and 1996 suggest an inverse relationship between the amplitude of eddy variability to the east and west of the plateau (see Plate 3b).

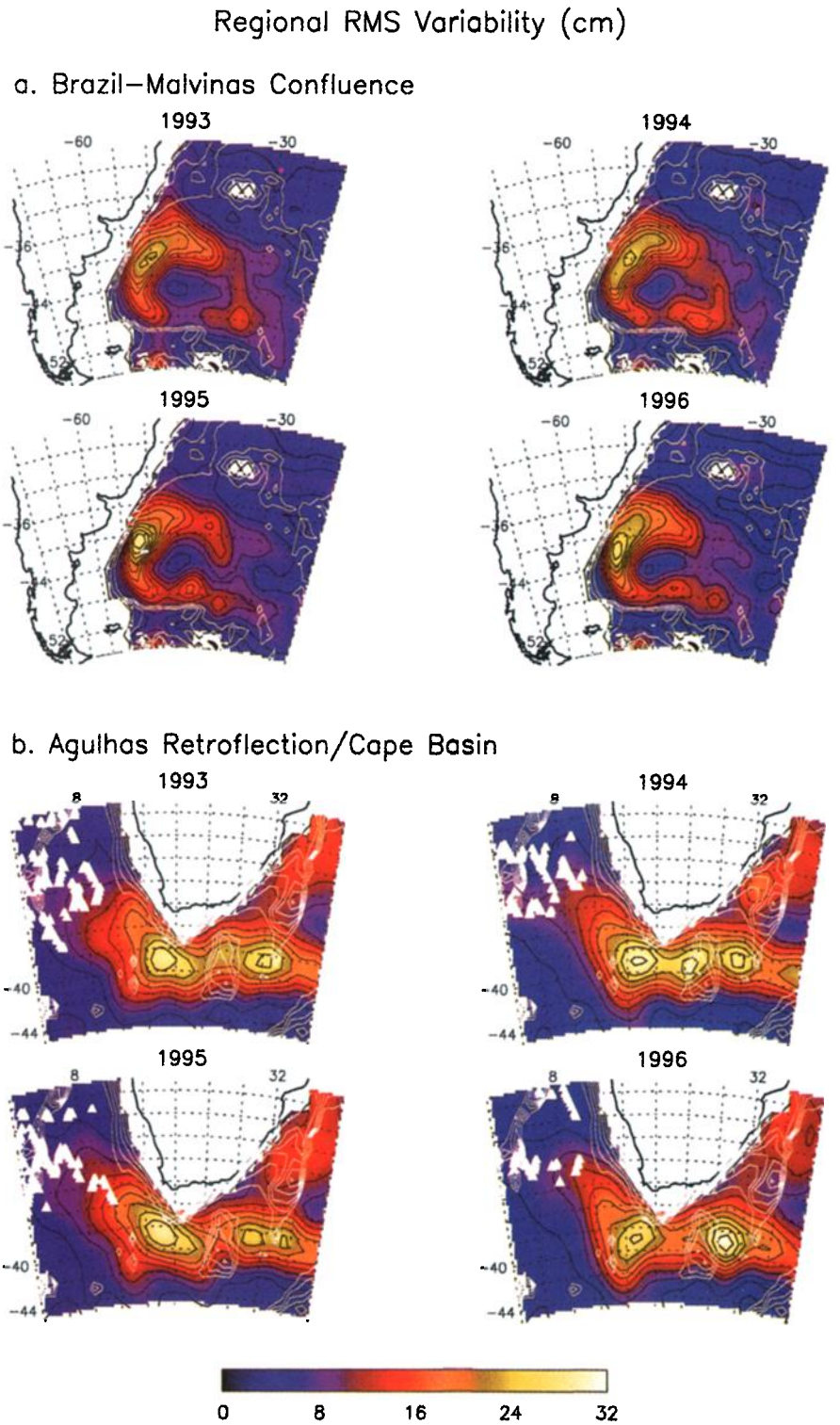

Plate 3. Year-to-year changes of rms variability in the (a) western and (b) eastern boundary regions of the South Atlantic (color image and contours). The contour intervals is 2 centimeters in the western boundary region and 3 centimeters in the eastern boundary region. Bathymetry contours are shown in white at 500 meter intervals. Near the eastern boundary, Agulhas eddy locations identified from the along-track data are plotted as triangles.

Such variations could result from low-frequency shifts in the longitude of the retroflection or from time-dependent variations in the stability of the Agulhas Return Current.

Model studies suggest that variability in the longitude of the retroflection results from either variations of Agulhas Current transport [*Ou and de Ruijter,* 1986] or from the influence of Natal Pulses on the trajectory of the Agulhas Current [*Lutjeharms and van Ballegooyen,* 1988]. Any such variations in the longitude of the retroflection may affect the eddy field. For example, the Agulhas Plateau may act as a barrier to the westward propagation of eddies formed at an "early" retroflection. Alternatively, the Agulhas Current may retroflect more smoothly and generate fewer eddies when it undergoes an early retroflection. Analysis of satellite SST imagery and drifter observations, with particular emphasis on the relationship between the longitude of the retroflection and the formation of Agulhas eddies, would clarify any such relationship. Detecting time-dependent variations of Agulhas Return Current stability and resolving the relationship between the stability of the Agulhas Return Current and other aspects of circulation at the retroflection would require a more intensive observational effort.

5. Westward Propagation

Unlike variability at the energetic boundary current regions, mesoscale variations are weaker at the interior of the gyre. The two most significant processes contributing to sea level changes in this relatively quiet zone are Rossby wave propagation [*Le Traon and Minster,* 1993; *Chelton and Schlax,* 1996] and the propagation of Agulhas eddies from the retroflection into the western South Atlantic [*Gordon and Haxby,* 1990; *Byrne et al.,* 1995; *Gründlingh,* 1995; *Goni et al.,* 1997]. Rossby wave propagation is easily visualized in longitude-time diagrams constructed from the gridded data. (Note that the first paper describing Rossby wave propagation from T/P observations used this same 6° loess smoother; see *Chelton and Schlax* [1996]). West of the Cape Basin, Agulhas eddies are best observed in the along-track data (see section 6); these eddies have smaller spatial scales and are typically attenuated by 60–80% by the 6° smoother.

Wave propagation is assessed from time-longitude plots of gridded T/P observations for a broad range of latitude within the South Atlantic basin. The 6° smoother was applied to the T/P observations to obtain sea level fields with statistically spatially uniform error distributions. Previous studies have identified strong semiannual Rossby waves signals in the South Atlantic subtropical gyre [*Le Traon and Minster,* 1993]. To emphasize variability on other timescales, we removed an annual and semiannual harmonic from the sea level time series at each location after gridding the data.

Between 35°S and 45°S, the largest amplitude variability is confined to the boundary current regions. In the example shown for 41°S (Plate 4a), high-amplitude variations are observed near the Cape Basin, in the Brazil-Malvinas Confluence, and in the offshore extension of the Brazil Current. At interior longitudes, very low-frequency variations, with little evidence of clear propagation, dominate the sea level anomaly fields. Similar variations are not observed in filtered SST records. Thus it is likely that this signal is of dynamic, rather than steric, origin. A comparison of the longitude–time diagram along 41°S and basin-scale EOF mode 1 (Plate 1) shows that the decrease of sea level along 41°S between 1993 and 1996 agrees well with the trend toward lower sea levels in basin-scale EOF mode 1 (Plate 1). This result suggests that low-frequency sea level variations in Plate 4a arise from dynamic shifts of circulation at the southern boundary of the gyre.

Between 24°S and 33°S, sea level variations associated with westward propagation across the interior of the gyre are the most prominent signal (Plates 4b and 4c). Particularly clear examples include the minimum of sea level (purple shading) at 0° longitude in early 1993 at 25.7°S. Along 25.7°S, the waves corresponding to this minimum arrive at the western boundary during December 1994 and April 1995. Less rapid westward propagation occurs along 29.5°, where the two waves arrive during May 1995 and April 1996. While oscillations at any given location occur on timescales shorter than the annual cycle, interannual variability clearly results from low-frequency amplitude modulation of the propagating waves. A comparison of wave amplitudes at seasonal and nonseasonal timescales (not shown) demonstrates the importance of low-frequency variability in the subtropical South Atlantic. The largest Rossby waves in Plate 4 have amplitudes of 8-10 cm. For comparison, annual and semiannual Rossby wave amplitudes rarely exceed 4 cm in this region [also see *Le Traon and Minster,* 1993]. Note that a similar result has been detected in the subtropical South Pacific, where *Wang and Koblinsky* [1996] found that interannual wave amplitudes can be 40% larger than the amplitudes of higher-frequency waves.

The zonal continuity of wave crests and troughs across the basin indicates that Rossby wave propagation is not particularly sensitive to the underlying topography. The zonal variations of amplitude for some features does, however, suggest that topography plays a secondary role in South Atlantic wave dynamics. Wave amplitudes are slightly larger west of the Mid-Atlantic Ridge. A less pronounced increase of amplitude west of the Rio Grande Rise (i.e., west of 40°W in Plate 4b) points to a similar role for this topographic feature.

For comparison with other studies of Rossby wave propagation [e.g., *Chelton and Schax,* 1996; *Wang and Koblinsky,* 1996; *Killworth et al.,* 1997], westward propagation speeds were estimated from the gridded data at each location in the gyre interior. For each latitude, sea level time series were extracted at locations sepa-

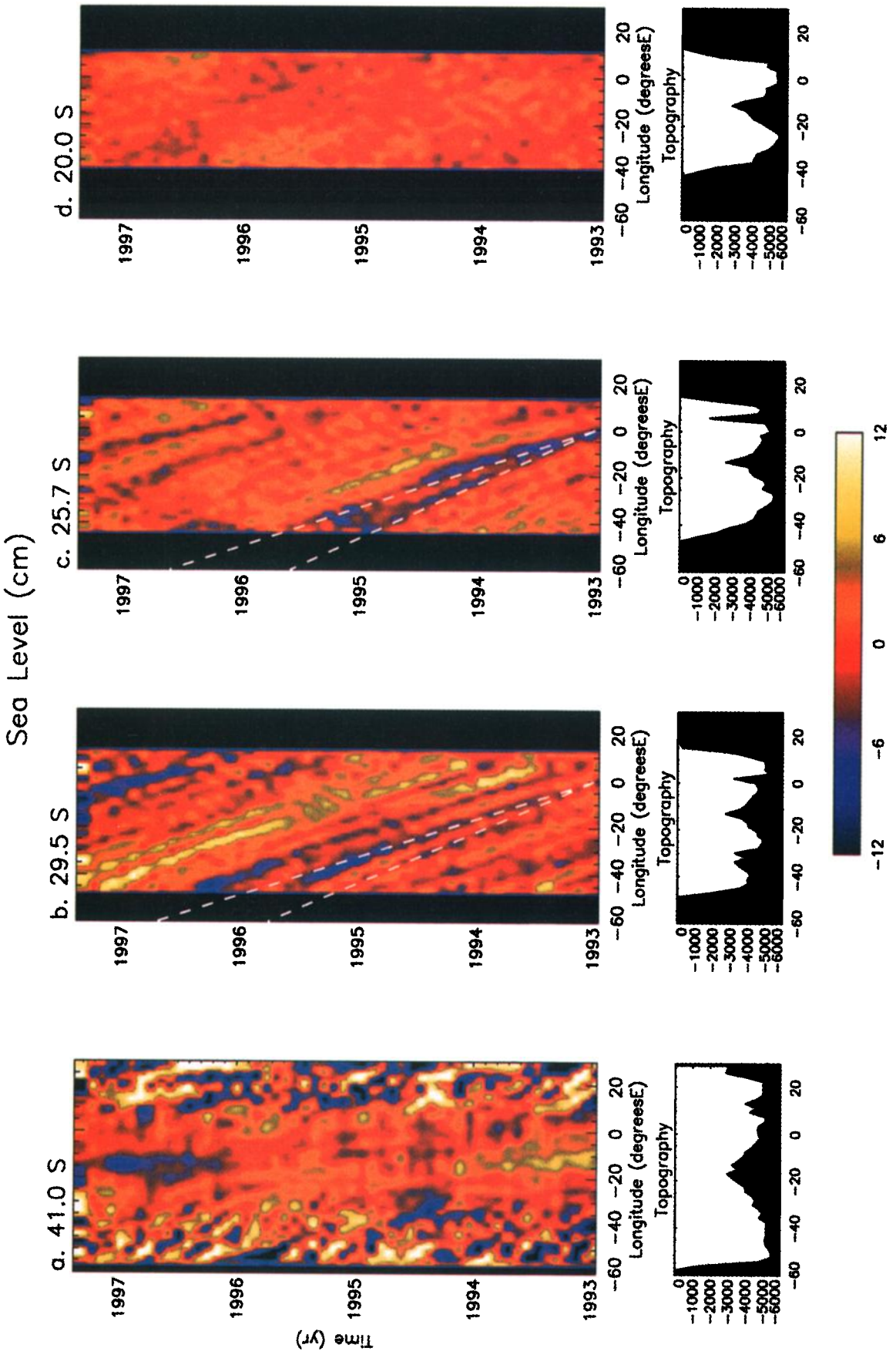

Plate 4. Longitude-time propagation diagrams for T/P sea level along four South Atlantic latitudes, (a) 41.0°S, (b) 29.5°S, (c) 25.7°S, and (d) 20.0°S. Lines corresponding to propagation speeds of 5.0 and 6.7 cm/s are shown in Plate 4b; lines corresponding to propagation speeds of 5.3 and 7.4 cm/s are shown in Plate 4c

rated by 3.8° longitude (two grid points in the zonal direction). The lagged cross correlation was computed for these time series, and the time lag that produced the strongest cross correlation was noted. Phase speed was then estimated based on the geographic distance between the two locations and the time lag of maximum cross correlation. The accuracy of the estimate was enhanced by (1) interpolating each time series to daily values prior to computing phase speed and (2) band passing each sea level time series to eliminate frequencies higher than one cycle per month and lower than one cycle per year. Subsequent calculations showed that phase speed estimates were not particularly sensitive to reasonable variations in the choice of passband. The quality of each phase speed estimate was gauged by the value of the cross correlation at the time of maximum lag. Cases with correlation values of 0.45 or larger resulted in phase speed estimates that were in good agreement with estimates at nearby locations. Smaller correlations were observed in cases where the time evolution of sea level at the two locations did not conform well to a simple model of westward propagation. An example of phase speed estimates along latitude 29.5°S is shown in Figure 6a. The gradual decrease of phase speed to the east is in good agreement with the reduction of phase speed associated with the shoaling of the thermocline toward the eastern side of the basin [*Killworth et al.*, 1997]. Figure 6b illustrates the relationship between phase speed estimates for this latitude and the cross-correlation coefficient; outliers, characterized by unrealistically large westward phase speed estimates, have low cross-correlation coefficients.

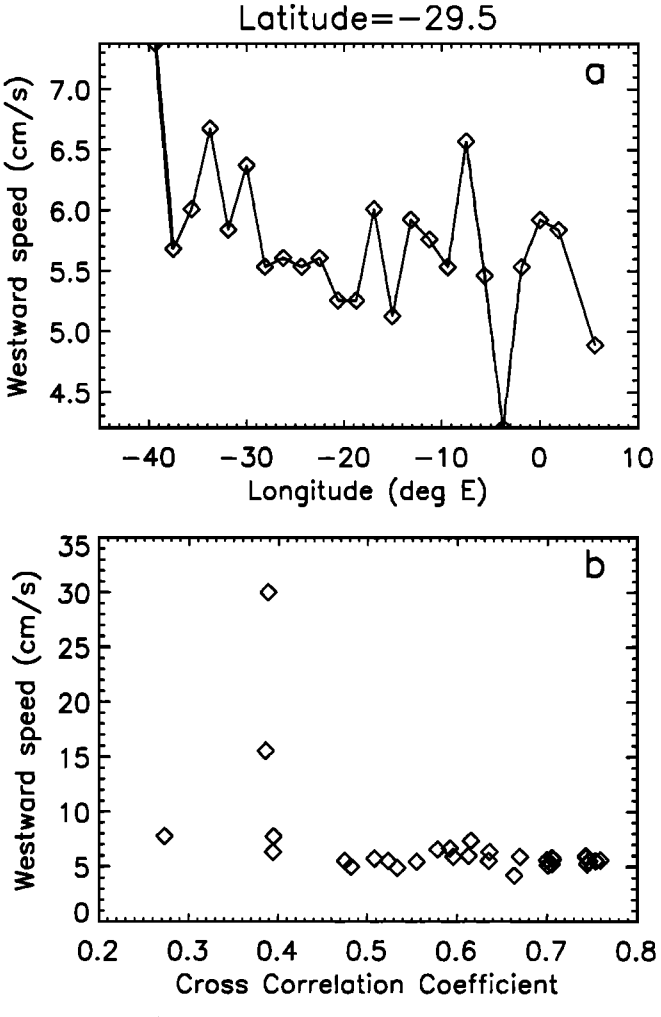

Figure 6. (a) Estimates of phase speed computed along latitude 29.5°S (see section 6 for a description of the method). (b) Phase speed estimates along 29.5°S plotted as a function of the maximum lagged cross correlation between the two time series used to compute phase speed (see section 6). Note the increase of noise in the phase speed estimates as the cross correlation decreases. Cases with small cross correlations are poorly described by a model of simple westward propagation.

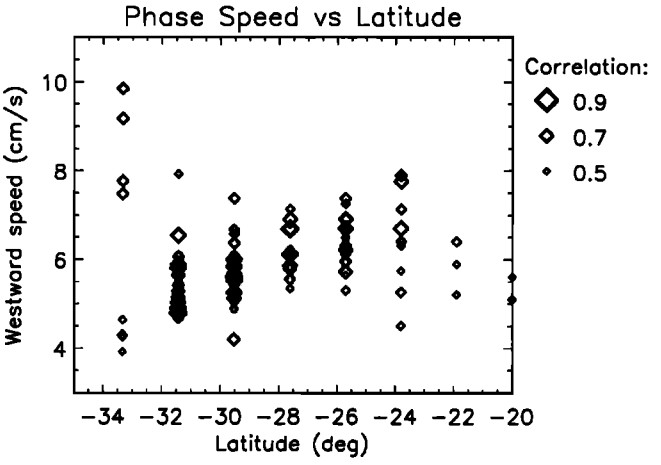

Figure 7. Westward phase speed estimates computed for the South Atlantic subtropical gyre and plotted as a function of latitude. The size of each symbol indicates the maximum lagged cross correlation between the two time series used to produce the estimate; larger symbols represent cases with higher-quality estimates. The range of phase speed estimates obtained for a given latitude is the result of noise in individual estimates as well as systematic variations of phase speed across the basin (also see Figure 6a).

The resulting phase speed estimates are shown as a function of latitude in Figure 7. South of 33°S, point-to-point noise in the phase speed estimates and the generally low cross-correlation values indicate that the dominant variability is not associated with wave propagation. This is in good qualitative agreement with visual inspection of longitude-time diagrams for these latitudes (e.g., Plate 4a). Between 33° and about 24°, the equatorward increase of phase speed is consistent with a Rossby wave propagation regime. Scatter in the phase speed estimates for particular latitudes within this band is the result of noise in the estimates, as well as systematic trends across the basin associated with the shoaling of the thermocline (see Figure 6a). The meridional gradient of phase speed corresponds well with values predicted for South Atlantic midlatitudes after adjusting for effects of the large-scale circulation on the mean potential vorticity gradient [*Killworth et al.*, 1997]. The

phase speeds are, however, systematically larger than those predicted from the most recent theory.

Both the contribution of Rossby wave propagation to sea level variability and the rms amplitude of sea level variations decrease to the north (Plate 4d; also see Figure 5). Between 10°S and 22°S, the dominant sea level variations are basin-scale features. There is little evidence of propagating interannual Rossby waves; the low-frequency variability north of the subtropical gyre has small amplitudes and is poorly organized.

6. Eddy Propagation

As noted above, a particularly unique aspect of South Atlantic ocean variability is the westward propagation of eddies from the Agulhas Retroflection into the South Atlantic subtropical gyre. In situ analyses have concluded that Agulhas eddies contribute significantly to the interbasin exchange of heat and salt [*Gordon et al.*, 1992; *Schmitz*, 1995]. Because many Agulhas eddies are trapped and spin down within the Cape Basin, these features fundamentally alter the water mass properties of the Benguela Current [*Duncombe Rae et al.*, 1996]. However, a significant fraction of Agulhas eddies also migrate across the Walvis Ridge, albeit in an attenuated form [*Byrne et al.*, 1995]. Estimates of the eddy contribution to the salt and vorticity budgets of the South Atlantic subtropical gyre indicate that these long-lived eddies play an active role in gyre dynamics [*Byrne et al.*, 1995]. Low-frequency variability in the flux of Agulhas eddies must therefore be considered when assessing interannual variations of gyre-scale circulation. Quantifying interannual variability of Agulhas eddy propagation is understandably difficult with the short data sets available prior to the launch of T/P. The 4 years of T/P data analyzed here provide the first evidence of interannual variations in the properties of Agulhas eddies at the interior of the gyre.

Agulhas eddies are readily identified in along-track altimeter observations based on their strong sea level signatures; anticyclonic circulation about an eddy produces a positive sea level anomaly, relative to the surrounding waters [*Gordon and Haxby*, 1990; *Byrne et al.*, 1995; *Gründlingh*, 1995; *Goni et al.*, 1997]. Unlike sea level anomalies associated with Rossby waves, Agulhas eddies have small spatial scales (i.e, diameters of 200–400 km) and exponentially decaying amplitudes as they spin down while propagating across the subtropical South Atlantic. Agulhas eddies have been successfully identified and tracked in Geosat observations of the South Atlantic [*Gordon and Haxby*, 1990; *Byrne et al.*, 1995], in T/P observations of the Cape Basin [*Goni et al.*, 1997], and in the first year of T/P observations of the South Atlantic basin [*Gründlingh*, 1995]. For this study, we tracked Agulhas eddies from the Cape Basin, across the Walvis Ridge, and into the interior of the subtropical gyre using a semiautomated version of the technique described by *Byrne et al.* [1995]. Data from the ascending and descending tracks were analyzed separately to enhance the robustness of the identifications. Only features that had consistent sea level amplitudes, spatial scales, and trajectories in both subsets of the along-track data were considered in this analysis. Candidate eddies were subject to secondary screening criteria to eliminate weak signals or features that were observed for short time intervals; only features that were observed for more than 6 months and that traveled over more than 10° of longitude or 5° of latitude were retained. In addition, we required that each feature be observed crossing the Walvis Ridge, except in two cases, where strong signals with properties characteristic of Agulhas eddies were detected just west of the Walvis Ridge at the beginning of the T/P record.

A total of 21 large-amplitude, long-lived eddies were identified for the period from December 1992 to May 1997. These identifications represent a lower bound on the actual propagation of Agulhas eddies into the South Atlantic subtropical gyre. The periods over which each eddy was tracked and the time at which the eddy crossed the Walvis Ridge are shown in Figure 8. Also shown in Figure 8 is a quantitative measure of our confidence in the eddy tracking procedure. For each time, the shading in Figure 8 depicts the amplitude of the eddy measured from the along-track data divided by the rms variability of sea level (excluding the eddy) within 3° latitude of the center of the eddy. Time-dependent variations of eddy confidence arise owing to separations between the center of the eddy and the ground track location and to time-dependent variations of eddy amplitude and background noise level. The average confidence index for all data shown in Figure 8 is 2.8, indicating that most of the eddies tracked were several times larger than the neighboring noise field.

Excluding eddies that were first observed at cycle 9 or last observed at cycle 171, each eddy was tracked for an average of 1.7 years over which it translated by 23.6° of longitude and 5.0° of latitude. Over this period, the decay in amplitude observed as eddies moved westward averaged 12.8 cm. Although seasonal variations have been observed in the Agulhas Current transport [*Ffield et al.*, 1997], similar variability is not apparent in the dynamical properties of eddies tracked from altimeter observations. Eddy properties, including amplitude, propagation speed, and diameter showed no systematic seasonal variations.

Figure 8 demonstrates that the observed eddy crossings of the Walvis Ridge are aperiodic. This may be due, in part, to aperiodic shedding of Agulhas eddies at the retroflection [see *Goni et al.*, 1997]. While eddies crossed the Walvis Ridge, on average, once every 75 days (4.8 eddies per year), there are two intervals during which successive eddy crossings are separated by 140 days or more. On three occasions, near-simultaneous crossings of two eddies are observed. The eddy locations inferred from the along-track data in these cases indicate that the centers of the eddies were separated by

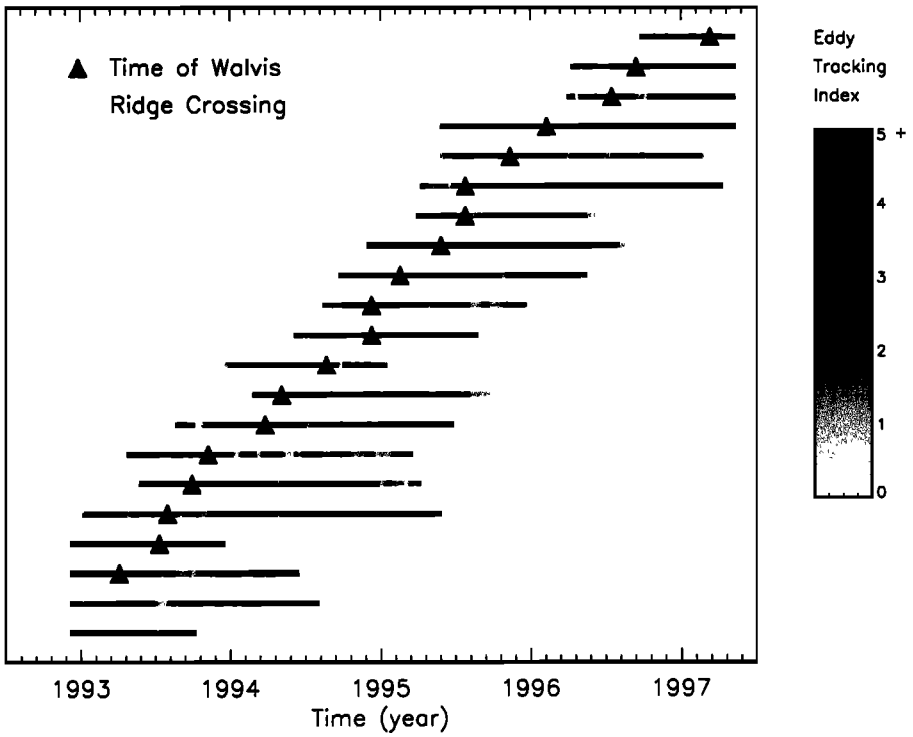

Figure 8. Agulhas eddies extracted from T/P along-track data. Each eddy is depicted by a horizontal bar. The position of the bar along the x axis corresponds to the time interval over which the eddy was tracked. At each time, the shading on the bar corresponds to the ratio between the eddy amplitude and the amplitude of variability in a region within 3° latitude and longitude of the eddy. Darker shades correspond to better eddy-tracking conditions. The triangles show the time at which each eddy crossed the Walvis Ridge. Note that the first two eddies crossed the Walvis Ridge before the beginning of the data set.

2.5°–4.4° of latitude as they crossed the ridge. The frequency of eddies entering the South Atlantic subtropical gyre in this study is lower than the six per year inferred by *Byrne et al.* [1995] from the Geosat observations. Five eddy crossings per year were observed during 1993, 1994, and 1995; only three eddies were observed crossing the ridge in 1996. It is difficult to ascertain whether the rate at which eddies entered the subtropical gyre is different for the Geosat and T/P sampling periods owing to differences in the sampling and quality of these two data sets. Analysis of other altimeter data sets (e.g., ERS 1, ERS 2, or Geosat follow-on) may provide insight on this issue.

The range of latitude and longitude over which Agulhas eddies are detected is generally referred to as the "Agulhas eddy corridor" [*Garzoli and Gordon,* 1996]. During the Geosat Exact Repeat Mission, the Agulhas eddy corridor was located between 25°S and 35°S for longitudes west of the Walvis Ridge [see *Byrne et al.*, 1995]. The Geosat data set was, however, too short to detect any systematic temporal variations in the migratory paths of the eddies. The longer sampling interval available from T/P reveals that the location of the Agulhas eddy corridor may vary on interannual timescales (see Figure 9). During 1993 and 1994, eddies propagated from the Cape Basin into the interior of the gyre over a broad range of latitudes. A very different situation occurred during 1996, when only one decaying feature was observed at the interior of the gyre south of 30°S. The eddy trajectories therefore indicate that the southern boundary of the eddy corridor shifted to the north between 1994 and 1996.

During the same period, a smaller southward shift of the northern boundary of the corridor also appears possible, based on the eddy trajectories in Figure 9. In the early part of the record, eddies located west of 0° have a strong northward component to their motion. This northward component is reduced or reversed in 1996. Unfortunately, it is difficult to assess whether this tendency represents a true southward shift of the northern boundary of the corridor or whether it is an artifact of the small number of eddies observed in the northwest quadrant of the domain. The larger number of eddy tracks in the eastern part of the gyre clearly indicates that the southern boundary of the eddy corridor shifted to the north during 1995.

7. Discussion

The interannual variations of the eddy corridor shown in Figure 9 may be a direct response to variations of the large-scale ocean circulation. As noted in section 3, the first basin-scale EOF mode corresponds to relatively large westward velocities in the eastern part of

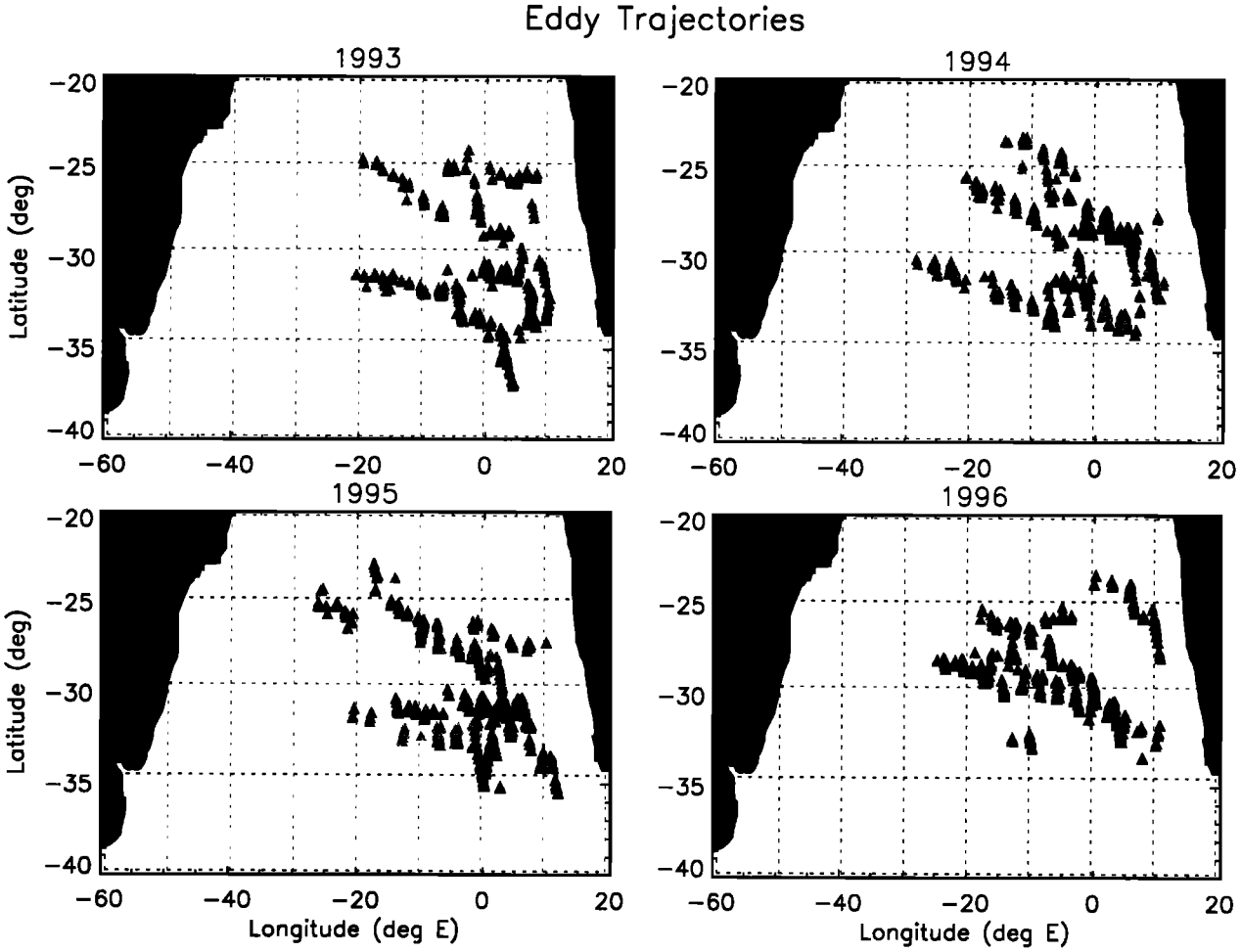

Figure 9. Agulhas eddy trajectories computed from the T/P data for 1993, 1994, 1995, and 1996. The observed location of each eddy is marked with a symbol; each eddy is plotted as a different shade. Note the change from a broad Agulhas eddy corridor for 1993 and 1994 to a narrower corridor in 1996. In 1996, the eddy near 10°E, 25°S was detected late in the year and may suggest a return to a broader eddy corridor in 1997.

the gyre during 1993 and 1994, followed by a transition to more sluggish westward velocities in 1996. This point can be illustrated more directly from the time series of zonal and meridional geostrophic velocity anomalies reconstructed from basin-scale mode 1 in the region between 10°W and 10°E (Figure 10). In this region, the time-mean flow is to the north and west (see Figure 1). Geostrophic velocity anomalies inferred from the filtered T/P data have particularly strong westward components during 1994. This reinforces the time-mean gyre circulation and coincides with the propagation of Agulhas eddies to the northwest. The tendency of eddies to propagate directly to the west is most pronounced in 1996. At this time, Figure 10 shows that eastward velocity anomalies oppose the westward component of the time-mean flow. As a result, advection by the large-scale gyre is anomalously weak.

A second possible link between the trajectories of the eddies and the large-scale gyre circulation is that motions on the two scales may be sensitive to a common forcing mechanism. For example, interactions between the Agulhas Current and the South Atlantic Current may affect the thermohaline and vorticity properties of the eddies near their region of formation, as well as the large-scale circulation of the gyre. Such relationships have not been observed in the in situ observations, although most analyses have focused on shorter spatial and temporal scales.

The dynamics of interactions between the eddies, the gyre-scale circulation, and the regional wind field cannot be conclusively evaluated from the observations used in this study. Analysis of covariability between sea level and the near-surface wind based on singular value decomposition (SVD) does, however, suggest a possible mechanism for the variations of gyre-scale circulation associated with sea level mode 1 (see Plate 1). SVD has been used previously to identify modes of sea level pressure and sea surface temperature covariability in the South Atlantic basin [*Venegas et al.*, 1997]. This method extracts spatial patterns of covariability in two fields by maximizing the mean square temporal covariance explained by the sequence of SVD spatial patterns

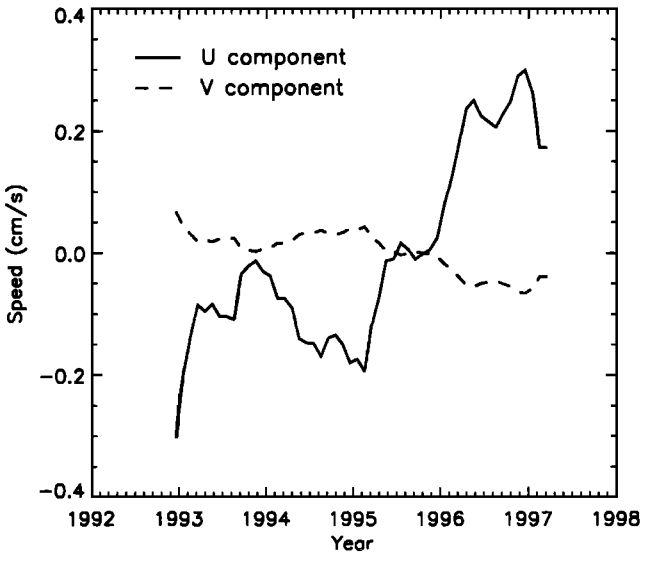

Figure 10. Anomalies of zonal (solid line) and meridional (dashed line) geostrophic velocity components reconstructed from the first EOF of basin-scale sea level variability (see Plate 1). Velocity components are averaged in a region northwest of the Cape Basin (10°W–10°E, 20°S–30°S). The time-mean flow in this region is to the northwest (see Figure 1). Negative zonal velocity anomalies reinforce the zonal component of time-mean flow; positive zonal velocity anomalies oppose the zonal component of the time-mean flow.

[see *Bretherton et al.*, 1995]. It is important to recognize that, while SVD is helpful for isolating relationships between variables, SVD does not conclusively establish cause and effect relationships; analysis of carefully designed model experiments is more suited to this task. The SVD method is, however, useful for preliminary analysis of possible links between observed fields.

Covariability between variations of gyre-scale sea level and variations of regional wind were evaluated based on SVD of T/P sea level observations (see section 2) and contemporaneous, monthly, near-surface zonal wind fields from the NCEP reanalysis [*Kalnay et al.*, 1996]. Prior to computing the SVD modes, the zonal wind fields were smoothed to eliminate small-scale variability and an annual harmonic was removed at each location. Because the wind field contains significant variability on semiannual timescales, a semiannual harmonic was removed from both the zonal wind and sea level fields prior to the SVD analysis. The resulting data sets emphasize variability on the interannual timescales of interest to this study.

As shown in Plate 5, the first mode of sea level and zonal wind covariability explains 31% of the mean square temporal covariance. The spatial correlation between the pattern of sea level from SVD mode 1 and the pattern of sea level from gyre-scale EOF 1 is remarkably strong (0.94). This high correlation suggests that the zonal wind pattern shown in Plate 5 (top left) is associated with the gyre-scale sea level variations discussed in section 2 and, possibly, with the year-to-year variations of Agulhas eddy trajectories discussed in section 6.

To further explore the possible link between variations of gyre-scale circulation and variations of the wind, a quantity somewhat analogous to the contribution of the mode 1 zonal wind pattern to the zonal component of wind stress curl is plotted in Plate 6. (Note that the actual contribution of zonal wind mode 1 to the true wind stress curl is not calculated here. This calculation requires an estimate of interannual variations in near-surface atmospheric stability. In the South Atlantic, these observations are considerably less reliable than observations of the wind components alone.) The field plotted in Plate 6 suggests that interannual variations of gyre-scale circulation are associated with variations in the large-scale wind stress curl. During 1993 and 1994, the zonal wind variability of SVD mode 1 (Plate 5, top left) opposes the time-mean wind pattern and the large-scale positive wind stress curl (Plate 6) is reduced. In 1996, the zonal wind variability of SVD mode 1 reinforces the time mean wind pattern and the large-scale positive wind stress curl is increased.

The anomaly pattern shown in Plate 6 can be compared with wind stress anomalies considered in previous studies of the wind-forced circulation of the South Atlantic basin. Simulations of seasonal variations of South Atlantic circulation demonstrate that the intensity of circulation about the gyre and the zonal extent of the gyre-scale circulation are sensitive to variations of wind stress curl [*Matano et al.*, 1993]. In a simulation of wind-driven gyre-scale circulation, the zonally averaged wind stress curl at 40°S and the Brazil Current transport were largest during austral spring and summer. At the same time, circulation in the western part of the basin was most intense and relatively weak circulation was observed in the eastern third of the basin [see *Matano et al.*, 1993, Figures 1–3]. As the zonally averaged wind stress curl weakened in austral fall and winter, circulation in the western part of the basin relaxed and exchange between the eastern and western sides of the basin increased. The spatial pattern of seasonal variations of gyre-scale circulation obtained by *Matano et al.* [1993] correspond remarkably well with the interannual variations of gyre-scale circulation isolated in the leading-order EOF mode (Plate 1, top). In addition, the relationship between the wind and the gyre-scale circulation inferred from T/P and the atmospheric reanalysis is qualitatively similar to the relationship obtained from numerical model simulations of the seasonal cycle. These inferences suggest that the dynamics governing large-scale South Atlantic circulation may be qualitatively similar on seasonal and interannual timescales. An important aspect of the interannual variability, which has no apparent analog in the seasonal cycle, is the potential link with water mass transport across the South Atlantic basin via Agulhas eddy propagation. The dynamics of this possible interaction will

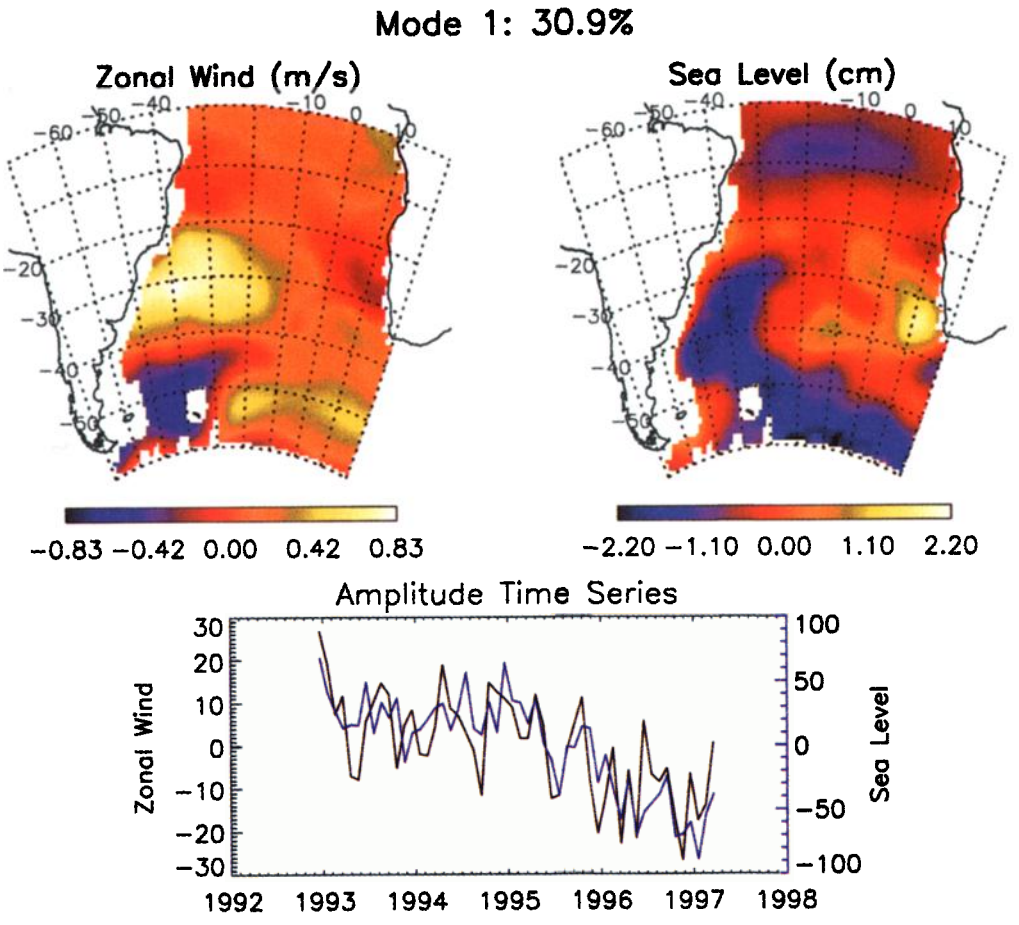

Plate 5. Leading mode of basin-scale zonal wind and sea level covariability computed from singular value decomposition. The spatial patterns of (top left) zonal wind and (top right) sea level are shown as color images. (bottom) Corresponding time series (zonal wind in black, sea level in purple). Zonal wind and sea level fields in Plate 5 (top) are plotted when the amplitude time series are equal to 10 and 30, respectively.

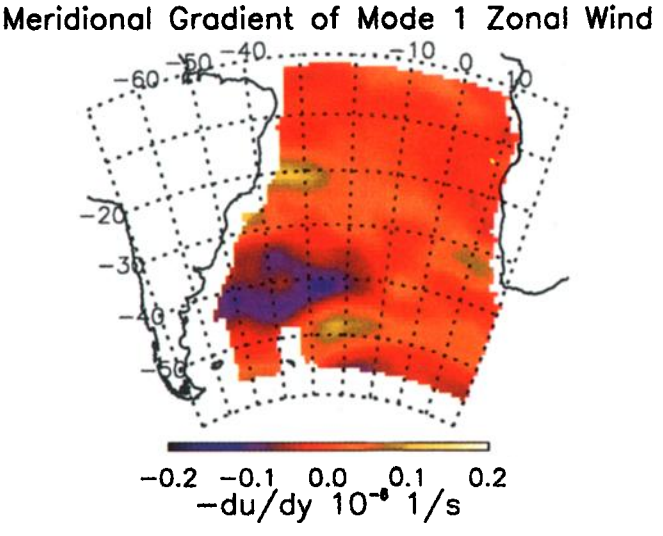

Plate 6. Negative of the meridional gradient of the zonal wind pattern shown in Plate 5.

be investigated in the next phase of this study using numerical experiments. Analysis of additional years of altimeter data are also expected to shed light on this potentially important aspect of South Atlantic wind-driven circulation.

8. Summary and Conclusions

In this study, we have analyzed interannual variability of the South Atlantic subtropical gyre and the regional circulation near the eastern and western boundaries using 4 years of TOPEX/POSEIDON sea level observations. The results demonstrate that a significant fraction of the total variability occurs at frequencies lower than the annual cycle. This is true of both the large-scale gyre circulation and of smaller-scale variations associated with the boundary current regimes.

Two particularly interesting modes of variability have been isolated. A basin-scale mode, which corresponds to zonal shifts in the dome of sea level associated with the subtropical gyre, accounts for more than half of the nonseasonal South Atlantic sea level variability. This mode suggests that there was a transition in 1995 from a broad, flat gyre with weak western boundary current transport, to a more zonally compact gyre, with stronger boundary flow. Variations in the strength of the geostrophic circulation in the northeastern part of the gyre associated with this mode may play a role in the dispersal of Agulhas eddies across the South Atlantic. Eddies propagate to the northwest in years where the gyre extends farther east. Eddies travel westward when the gyre is displaced to the west. Calculations of sea level and zonal wind covariability based on singular value decomposition suggest that this mode of ocean circulation may be linked to variations of the large-scale zonal wind field. Numerical experiments will be needed to evaluate the dynamics of this relationship and to investigate the degree to which Agulhas eddies are affected by variations of the large-scale wind forcing and by low-frequency variations of gyre-scale circulation.

A second mode of interannual variability was identified in the Brazil-Malvinas Confluence region. This mode corresponds to meridional variations of the latitude of the confluence and to variations in the local distribution of eddy variability. Variations in this mode occur on timescales of 2–3 years. Sea level fields indicate that this mode is linked to time-dependent changes of the surface velocity of the Malvinas Current. The maximum of eddy variability is intense and spatially compact when the modal analysis suggests that the Malvinas Current is anomalously weak and the confluence is displaced to the south. In years when the confluence is displaced to the north, the region of high variability is more geographically dispersed and variability is much larger along the offshore extension of the Brazil Current.

The optimistic outlook for the continued operation of the T/P satellite and the anticipated launch of other satellite altimeters indicate that detecting and interpreting variations of ocean circulation on interannual and longer timescales will be a primary focus of future altimetric investigations. Long data sets, such as that available from T/P, are essential for resolving interactions between ocean processes on a broad range of spatial scales. A particular advantage of satellite altimetry is its ability to resolve low-frequency variations of basin-scale circulation, as well as low-frequency variations in the statistics of mesoscale variability. Few in situ data sets have the spatial coverage and temporal resolution needed for studies of multiscale ocean interactions on interannual timescales.

A principal result of this study is the isolation of links between large-scale and mesoscale variability of South Atlantic circulation. This variability may contribute to low-frequency changes of the water mass properties of the basin and to changes of South Atlantic dynamics on interannual timescales. Questions regarding these larger issues will be addressed as additional altimeter data are collected and in a planned series of numerical process studies.

Acknowledgments. We thank Victor Zlotnicki and Akiko Hayashi (Jet Propulsion Laboratory, California Institute of Technology) for making their gridded TOPEX/-POSEIDON altimeter residuals available for this investigation; their residuals were based on the MGDR from the NASA Physical Oceanography Distributed Active Archive Center (PO-DAAC). The research described here was supported by grant JPLCIT 96-0865 from the Jet Propulsion Laboratory funded under the TOPEX/POSEIDON Extended Mission Announcement of Opportunity. Lamont-Doherty Earth Observatory contribution 5902.

References

Bretherton, C. S., C. Smith, and J. M. Wallace, An intercomparison of methods for finding coupled patterns in climate data, *J. Clim., 5,* 541–560, 1995.

Byrne, D., A. L. Gordon, and W. Haxby, Agulhas eddies: A synoptic view using Geosat ERM data, *J. Phys. Oceanogr., 25,* 902–917, 1995.

Chelton, D. B., and M. G. Schlax, Global observations of oceanic Rossby waves, *Science, 272,* 234–238, 1996.

Chelton, D. B., M.G. Schlax, D. L. Witter, and J. G. Richman, Geosat altimeter observations of the surface circulation of the Southern Ocean, *J. Geophys. Res., 95,* 17,877–17,903, 1990.

Deser, C., M. A. Alexander, and M. S. Timlin, Upper-ocean thermal variations in the North Pacific during 1970–1991, *J. Clim., 9,* 1840–1855, 1996.

Duncombe Rae, C. M., Agulhas Retroflection rings in the South Atlantic Ocean: An overview, *S. Afr. J. Mar. Sci., 11,* 327–344, 1991.

Duncombe Rae, C. M., S. L. Garzoli, and A. L. Gordon, The eddy field of the southeast Atlantic Ocean: A statistical census from the Benguela Sources and Transport project, *J. Geophys. Res., 101,* 11,949–11,964, 1996.

Ffield, A., J. Toole, and D. Wilson: Seasonal circulation in the South Indian Ocean, *Geophys. Res. Lett., 24,* 2773–2776, 1997.

Forbes, C., K. Leaman, D. Olson, and O. Brown, Eddy and wave dynamics in the South Atlantic as diagnosed from Geosat altimeter data, *J. Geophys. Res., 98,* 12,297–12,314, 1993.

Fu, L.-L., The circulation and variability of the South Atlantic Ocean: First results from the TOPEX/POSEIDON mission, in *The South Atlantic: Present and Past Circulation*, edited by G. Wefer et al., pp. 63–82, Springer-Verlag, New York, 1996.

Fu, L.-L., E. J. Christensen, C. A. Yamarone, M. Lefebvre, Y. Ménard, M. Dorrer, and P. Escudier, TOPEX/-POSEIDON mission overview, *J. Geophys. Res., 99,* 24,369–24,382, 1994.

Garzoli, S. L., Geostrophic velocity and transport variability in the Brazil-Malvinas Confluence, *Deep Sea Res., Part I, 40,* 1379–1403, 1993.

Garzoli, S. L., and A. L. Gordon, Origins and variability of the Benguela Current, *J. Geophys. Res., 101,* 897–906, 1996.

Garzoli, S. L., G. J. Goni, A.J. Mariano, and D.B. Olson, Monitoring the upper southeastern Atlantic transports using altimeter data, *J. Mar. Res., 55,* 453–481, 1997.

Goni, G. J., S. L. Garzoli, A. J. Roubicek, D. B. Olson, and O. B. Brown, Agulhas ring dynamics from TOPEX/-POSEIDON satellite altimeter data, *J. Mar. Res., 55,* 861–883, 1997.

Gordon, A. L., Which is it: Warm or cold route, or maybe both?. Int. WOCE Newsl., vol. 28, pp. 33-34, WOCE Int. Proj. Off. at Southhampton Oceanogr. Cent., Southampton, England, 1997.

Gordon, A. L., and W. F. Haxby, Agulhas eddies invade the South Atlantic–Evidence from Geosat altimeter and shipboard CTD, *J. Geophys. Res., 95,* 3117–3125, 1990.

Gordon, A. L., R. F. Weiss, W. M. Smethie, and M. J. Warner, Themocline and intermediate water communication between the South Atlantic and Indian Oceans, *J. Geophys. Res., 97,* 7223–7240, 1992.

Greenslade, D. J. M., D. B. Chelton, and M. G. Schlax, The midlatitude resolution capability of sea level fields constructed from single and multiple satellite altimeter datasets, *J. Atmos. Oceanic Technol., 14,* 849–870, 1997.

Gründlingh, M. L., Tracking eddies in the southeast Atlantic and southwest Indian oceans with TOPEX/POSEIDON, *J. Geophys. Res., 100,* 24,977–24,986, 1995.

Kalnay, E. et al., The NCEP/NCAR 40-year reanalysis project, *Bull. Am. Meteorol. Soc., 77,* 437–471, 1996.

Killworth, P. D., D. B. Chelton, and R. A. deSzoeke, The speed of observed and theoretical long extratropical planetary waves, *J. Phys. Oceanogr., 27,* 1946–1966, 1997.

Le Traon, P.-Y., and J.-F. Minster, Sea level variability and semiannual Rossby waves in the South Atlantic subtropical gyre, *J. Geophys. Res., 98,* 12,315–12,326, 1993.

Lutjeharms, J., The exchange of water between the south Indian and South Atlantic Oceans. in *The Southern Atlantic: Present and Past Circulation*, edited by G. Wefer et al., pp. 125-162, Springer-Verlag, New York, 1996.

Lutjeharms, J. R. E., and J. Cooper, Interbasin leakage through Agulhas current filiments, *Deep Sea Res., Part I, 43,* 213–238, 1996.

Lutjeharms, J. R. E., and R. C. van Ballegooyen, The retroflection of the Agulhas Current, *J. Phys. Oceanogr., 18,* 1570–1583, 1988.

Matano, R. P., M. G. Schlax, D. B. Chelton, Seasonal variability in the Southwestern Atlantic, *J. Geophys. Res., 98,* 18,027–18,036, 1993.

Matano, R. P., C. G. Simionato, W. P. de Ruijter, P. J. van Leeuween, P. T. Strub, D. B. Chelton, and M. G. Schlax, Seasonal variability in the Agulhas Retroflection region. *Geophys. Res. Lett., 25,* 4361–4364, 1998.

McClean, J. L., A. J. Semtner, and V. Zlotnicki, Comparisons of mesoscale variability in the Semtner–Chervin 1/4° model, the Los Alamos Parallel Ocean Program 1/6° model, and TOPEX/POSEIDON data. *J. Geophys. Res., 102,* 25,203–25,226, 1997.

Olson, D. B., G. P. Podesta, R. H. Evans, and O. B. Brown, Temporal variations in the separation of Brazil and Malvinas currents, *Deep Sea Res., Part A, 35,* 1971-1990, 1988.

Ou, H. W., and W. P. M. de Ruijter, Separation of an inertial boundary current from a curved coastline, *J. Phys. Oceanogr., 16,* 280–289, 1986.

Pearce, A. F., and M. L. Gründlingh, Is there a seasonal variation in the Agulhas Current?, *J. Mar. Res., 40,* 177–184, 1982.

Peterson, R., and L. Stramma, Upper-level circulation in the South Atlantic, *Prog. Oceanogr., 26,* 1–73, 1991.

Preisendorfer, R. W., *Principal Component Analysis in Meteorology and Oceanography.* 425 pp., Elsevier, New York, 1988.

Provost, C., and P.-Y. Le Traon, Spatial and temporal scale in altimetric variability in the Brazil-Malvinas Current confluence region: Dominance of the semiannual period and large spatial scales, *J. Geophys. Res., 98,* 18,037–18,052, 1993.

Reid, J. L., On the total geostrophic circulation of the South Atlantic Ocean: Flow patterns, tracers and transports, *Prog. Oceanogr., 23,* 149–244, 1989.

Reynolds, R. W., and T. M. Smith, Improved global sea surface temperature analyses, *J. Clim., 7,* 929-948, 1994.

Schlax, M. G., and D. B. Chelton, Frequency domain diagnostics for linear smoothers, *J. Am. Stat. Assoc., 87,* 1070–1081, 1992.

Schlax, M. G., and D. B. Chelton, Aliased tidal errors in TOPEX/POSEIDON sea surface height data, *J. Geophys. Res., 99,* 24,761–24,775, 1994.

Schlax, M. G., and D. B. Chelton, Correction to "Aliased tidal errors in TOPEX/POSEIDON sea surface height data," *J. Geophys. Res., 101,* 18,451, 1996.

Schmitz, W. J., On the interbasin-scale thermohaline circulation, *Rev. Geophys., 33,* 151–173, 1995.

Stammer, D., Steric and wind-induced changes in TOPEX/-POSEIDON large-scale sea surface topography observation, *J. Geophys. Res., 102,* 20,987–21,009, 1997.

van Ballegooyen, R. C., M. L. Grundlingh, and J. R. E. Lutjeharms, Eddy fluxes of heat and salt from the southwest Indian Ocean into the southeast Atlantic Ocean: A case study, *J. Geophys. Res., 99,* 14,053–14,070, 1994.

Venegas, S. A., L. A. Mysak, and D. N. Straub, Atmosphere-ocean coupled variability in the South Atlantic, *J. Clim., 10,* 2904–2920, 1997.

Wang, L., and C. J. Koblinsky, Low-frequency variability in the region of the Agulhas Retroflection, *J. Geophys. Res., 101,* 3597–3614, 1996.

Whitworth, T., W. D. Nowlin, R. D. Pillsbury, M. I. Moore, and R. F. Weiss, Observations of the Antarctic Circumpolar Current and deep boundary current in the southwest Atlantic, *J. Geophys. Res., 96,* 15,105–15,118, 1991.

A. L. Gordon and D. L. Witter, Lamont-Doherty Earth Observatory, Columbia University, Route 9W, Palisades, NY 10964. (dwitter@ldeo.columbia.edu)

(Received May 20, 1998; revised December 8, 1998; accepted January 29, 1999.)